AGU PUBLICATIONS

Geochemistry, Geophysics, Geosystems

RESEARCH ARTICLE
10.1002/2014GC005527

Special Section:
Magnetism From Atomic to Planetary Scales: Physical Principles and Interdisciplinary Applications in Geo- and Planetary Sciences

Key Points:
- Titanomagnetite Curie temperatures are strongly dependent on thermal history
- Observations suggest time and temperature-dependent cation ordering
- This has important implications in paleomagnetism and geospeedometry

Correspondence to:
M. Jackson,
jacks057@umn.edu

Citation:
Jackson, M., and J. A. Bowles (2014), Curie temperatures of titanomagnetite in ignimbrites: Effects of emplacement temperatures, cooling rates, exsolution, and cation ordering, *Geochem. Geophys. Geosyst.*, *15*, 4343–4368, doi:10.1002/2014GC005527.

Received 28 JUL 2014
Accepted 31 OCT 2014
Accepted article online 6 NOV 2014
Published online 25 NOV 2014

Curie temperatures of titanomagnetite in ignimbrites: Effects of emplacement temperatures, cooling rates, exsolution, and cation ordering

Mike Jackson[1] and Julie A. Bowles[2]

[1]Institute for Rock Magnetism, Winchell School of Earth Sciences, University of Minnesota, Minneapolis, Minnesota, USA, [2]Department of Geosciences, University of Wisconsin–Milwaukee, Milwaukee, Wisconsin, USA

Abstract Pumices, ashes, and tuffs from Mt. St. Helens and from Novarupta contain two principal forms of titanomagnetite: homogeneous grains with Curie temperatures in the range 350–500°C and oxyexsolved grains with similar bulk composition, containing ilmenite lamellae and having Curie temperatures above 500°C. Thermomagnetic analyses and isothermal annealing experiments in combination with stratigraphic settings and thermal models show that emplacement temperatures and cooling history may have affected the relative proportions of homogeneous and exsolved grains and have clearly had a strong influence on the Curie temperature of the homogeneous phase. The exsolved grains are most common where emplacement temperatures exceeded 600°C, and in laboratory experiments, heating to over 600°C in air causes the homogeneous titanomagnetites to oxyexsolve rapidly. Where emplacement temperatures were lower, Curie temperatures of the homogeneous grains are systematically related to overburden thickness and cooling timescales, and thermomagnetic curves are generally irreversible, with lower Curie temperatures measured during cooling, but little or no change is observed in room temperature susceptibility. We interpret this irreversible behavior as reflecting variations in the degree of cation ordering in the titanomagnetites, although we cannot conclusively rule out an alternative interpretation involving fine-scale subsolvus unmixing. Short-range ordering within the octahedral sites may play a key role in the observed phenomena. Changes in the Curie temperature have important implications for the acquisition, stabilization, and retention of natural remanence and may in some cases enable quantification of the emplacement temperatures or cooling rates of volcanic units containing homogeneous titanomagnetites.

1. Introduction

The titanomagnetites, spinels of the magnetite-ulvöspinel solid-solution series ($Fe_{3-x}Ti_xO_4$ with $0 \leq x \leq 1$), are the most important naturally occurring magnetic materials [*Dunlop and Özdemir*, 1997, 2007; *Tauxe*, 2010]. They are the major carriers of natural remanent magnetization (NRM) in most terrestrial rocks and sediments, thereby providing critical information on geomagnetic field history and tectonic plate motions. Furthermore, they are commonly significant sources of magnetic anomalies [*Gee and Kent*, 2007; *Purucker and Whaler*, 2007], magnetic fabrics [*Martín-Hernández et al.*, 2004], and environmental magnetic signals [*Evans and Heller*, 2003; *Liu et al.*, 2012]. Despite their importance in rock magnetism, some important fundamental aspects of titanomagnetite mineral magnetism remain incompletely understood, especially concerning (a) the arrangement of cations in the crystal structure, changes in the cation distribution with temperature and time, and the effects of such changes on essential magnetic properties [e.g., *Creer and Stephenson*, 1972; *Lattard et al.*, 2006; *Pearce et al.*, 2010; *Lilova et al.*, 2012; *Bowles et al.*, 2013; *Harrison et al.*, 2013] and (b) the thermodynamic stability of the magnetite-ulvöspinel solid solution. Uncertainties in the latter relate to its dependence on temperature, oxygen fugacity (fO_2), composition (including substituted cations), and cation site occupancies [e.g., *Bowles et al.*, 2012; *Lattard et al.*, 2012; *Lilova et al.*, 2012].

Titanomagnetites crystallize in the spinel structure; a cubic framework of oxygen anions provides tetrahedrally coordinated (*A*) and octahedrally coordinated (*B*) sites, some fraction of which are occupied by metal cations. The unit cell comprises 32 oxygens, defining 64 tetrahedral sites, 8 of which are occupied, and 32 octahedral sites, 16 of which contain cations. Simple spinels contain two cationic species and have a generalized chemical formula AB_2O_4 (representing one eighth of the unit cell), where A and B can be divalent,

trivalent, or quadrivalent ions in charge-balanced proportions. Spinels are categorized as normal or inverse according to how these cations are distributed among the *A* and *B* sites: in a "normal" spinel the A cations reside exclusively in the *A* (tetrahedral) sites and the B cations occupy the *B* sites [e.g., *O'Neill and Navrotsky*, 1983, 1984]. For example, the mineral spinel (structural formula $Mg^{2+}[Al^{3+}{}_2]O_4$, where the square brackets denote octahedral site occupancy) has 8 Mg^{2+} and 16 Al^{3+} ions per unit cell; all the divalent A ions occupy tetrahedral *A* sites and all the trivalent B ions are in octahedral *B* sites, and this represents the "normal" arrangement for a 2–3 spinel (i.e., one with divalent A and trivalent B cations [*O'Neill and Navrotsky*, 1983, 1984]). In the "inverse" arrangement, the *A* sites contain B cations (half of them) and the A cations reside in the *B* sites along with the rest of the B cations. The end-members of the titanomagnetite solid solution series are both inverse spinels: magnetite ($x = 0$; $Fe^{3+}[Fe^{2+}Fe^{3+}]O_4$) and ulvöspinel ($x = 1$; a 4–2 spinel with structural formula $Fe^{2+}[Fe^{2+}Ti^{4+}]O_4$). In general, the degree of inversion (and order) for a simple 2-cation spinel may be represented by an inversion parameter *b*: $A_{1-b}B_b[A_bB_{2-b}]O_4$. A perfectly ordered normal spinel is represented by $b = 0$, a perfectly ordered inverse spinel by $b = 1$, and a perfectly random (disordered) distribution by $b = 2/3$. A related parameter used in some thermodynamic models [e.g., *Harrison and Putnis*, 1999b, 1999a] is the order parameter *Q*, which has a value of zero in the fully disordered state and positive and negative values, respectively, for normal and inverse ordering ($Q = X_B{}^{oct} - X_B{}^{tet} = 1–3b/2$, where $X_B{}^{oct}$ and $X_B{}^{tet}$ are, respectively, the fractions of octahedral and tetrahedral sites occupied by B cations).

Two important factors complicate the ideal ordered arrangement. First, the cation distribution is commonly temperature-dependent, becoming more random at elevated temperatures [*O'Neill and Navrotsky*, 1983, 1984; *Harrison and Putnis*, 1999b, 1999a]. Second, intermediate titanomagnetite compositions ($0 < x < 1$) have three cationic species (Fe^{2+}, Fe^{3+}, and Ti^{4+}), and additional cation substitution (e.g., Mg^{2+}, Al^{3+}) is common [e.g., *Creer and Stephenson*, 1972; *Richards et al*., 1973; *Nishitani*, 1981; *Ghiorso and Evans*, 2008]. Therefore, the number of possible ways to distribute the various cations into the *A* and *B* sites is large, and as a result the "usual" cation distribution and its temperature dependence remain incompletely known for the titanomagnetites [e.g., *O'Donovan and O'Reilly*, 1980; *Trestman-Matts et al*., 1983; *Moskowitz*, 1987; *Kakol et al*., 1991; *Wanamaker and Moskowitz*, 1994; *Hamdeh et al*., 1999; *Bosi et al*., 2009; *Lilova et al*., 2012]. The details of the cation site occupancy are important because they exert fundamental controls on the intrinsic properties of these key magnetic minerals.

Magnetic ordering in ferrimagnetic spinels is dominated by antiferromagnetic exchange interactions between *A*-site and *B*-site cations [*Néel*, 1948, 1955]. Two magnetic sublattices are thereby defined: the tetrahedral sublattice, with eight cations per unit cell, whose moments are mutually parallel; and the octahedral sublattice, with 16 cations per unit cell, whose mutually parallel moments are antiparallel to those of the tetrahedral site cations ("collinear antiferromagnetism"). Because the octahedral sublattice contains twice as many cations as the tetrahedral sublattice, a strong net spontaneous magnetization can result, but its strength depends on the atomic moments of the cations involved and their distribution into the *A* and *B* sites. For magnetite ($Fe^{3+}[Fe^{2+}Fe^{3+}]O_4$), the Fe^{3+} contributions to the *A*- and *B*-sublattice magnetizations are mutually canceling, and the net spontaneous moment per formula unit is equal to that of one Fe^{2+} ion, $4\mu_B$ (4 Bohr magnetons). Ulvöspinel ($Fe^{2+}[Fe^{2+}Ti^{4+}]O_4$) is a pure antiferromagnet (below its Néel temperature) with no net spontaneous magnetization. Between these end-members, the net moment of the sublattices depends on both *x* and *b*, as can be seen from the generalized structural formula $Fe^{2+}{}_{1-b}Fe^{3+}{}_b[Fe^{2+}{}_{b+x}Fe^{3+}{}_{2-2x-b}Ti^{4+}{}_x]O_4$ for $0 \leq x \leq 0.5$ (assuming that titanium is exclusively in the *B* site [e.g., *Wechsler et al*., 1984]). Experimental data show considerable scatter in the dependence of the saturation magnetization (M_S) upon *x*, and various models have been proposed for the underlying cation distributions [*Chevallier et al*., 1955; *Néel*, 1955; *O'Reilly and Banerjee*, 1965; *Kakol et al*., 1991; *Hamdeh et al*., 1999; *Bosi et al*., 2009; *Pearce et al*., 2010].

The Curie temperature also depends on cation distribution, but in a less directly quantitative way. Néel's model of $M_S(T)$, based on molecular field theory and modified by *Stephenson* [1972] to allow for two different species of magnetic cation (e.g., Fe^{2+} and Fe^{3+}), predicts a strong dependence of T_C on total concentration of magnetic ions but a relatively weak dependence on how they are distributed within the sublattices [*O'Reilly*, 1984]. *Creer and Stephenson* [1972] modeled the effects of varying cation distributions on T_C in titanomagnetites with $x \geq 0.4$ and having Al^{3+} and Mg^{2+} contents of up to 0.2 atoms per formula unit, and they predicted that differing degrees of order would generally cause changes in T_C of less than 20°C. However, experimental evidence from synthetic titanomagnetites [*Lattard et al*., 2006] and from synthetic

magnesioferrites ($Mg^{2+}_{1-b}Fe^{3+}_{b}[Mg^{2+}_{b}Fe^{3+}_{2-b}]O_4$) [*Harrison and Putnis*, 1999b, 1999a] suggests that these models dramatically underestimate the effects of cation ordering on T_C, probably due to associated effects including cation vacancies [*Lattard et al*., 2006] and the interaction of magnetic ordering and cation ordering [*Burton*, 1991; *Harrison and Putnis*, 1999b, 1999a; *Harrison et al*., 2013]. In magnesioferrite, there is a near-linear positive relationship between the cation order degree $|Q|$ and the Curie temperature [*O'Neill et al*., 1992; *Harrison and Putnis*, 1999b, 1999a]. Changes in T_C of up to 100°C can be produced in magnesioferrites by thermal treatments (annealing or quenching) that cause changes in the cation ordering [*Harrison and Putnis*, 1999b, 1999a].

Recently, we have demonstrated that the Curie temperature is strongly sensitive to the experimental thermal history in a set of natural homogeneous titanomagnetites from the pyroclastic deposits of historical eruptions of Mt. St. Helens (Washington State) and Novarupta (Alaska), and we interpreted this sensitivity in terms of time- and temperature-dependent cation ordering [*Bowles et al*., 2013], similar to that in the magnesioferrite system. Irreversible thermomagnetic curves, with heating-leg Curie temperatures exceeding those for the cooling leg by as much as 100°C, but with little or no change in the room-temperature susceptibility or saturation magnetization, suggest rapid disordering of the cation distribution at temperatures exceeding about 500°C. Thermal annealing of the same samples at 350°C or 400°C for time intervals ranging from 1 to 1000 h caused the Curie temperatures to increase again by as much as 100°C. This change in T_C (ΔT_C) scales proportionally with the logarithm of isothermal annealing time, suggesting slow approach to an equilibrium state of higher order in the cation distribution [*Bowles et al*., 2013]. Subsequent thermomagnetic measurements again exhibited the same sort of irreversibility as the untreated samples, and the cycle was found to be repeatable: ordering by annealing raises T_C and disordering at $T > 500$°C followed by relatively rapid cooling freezes in the disordered distribution with its reduced T_C.

A number of important aspects of this phenomenon remain unresolved, including the exact nature of the crystal-chemical changes responsible for raising and lowering T_C, the roles of substitute cations like Al^{3+} and Mg^{2+}, how commonly it occurs in natural titanomagnetites, and how it affects their paleomagnetic records. In this paper we present new data from additional annealing experiments on the same sample set from Mt. St. Helens and Novarupta, allowing us to refine the kinetics of the processes responsible for the sensitivity of Curie temperature to thermal history. In addition we present new data from additional Mt. St. Helens samples in stratigraphic context, which clearly demonstrate the strong dependence of T_C on cooling history. We examine all of the experimental results to characterize the dependence of T_C (and presumably of cation ordering) on emplacement temperatures and cooling history of the pyroclastic material and on composition of the titanomagnetites.

2. Geological Setting and Sampling

2.1. Novarupta 1912 Pyroclastic Eruptions, Valley of Ten Thousand Smokes (VTTS)

Approximately 11 km^3 of ash flows and 17 km^3 of air fall were deposited over a 60 h period in 1912 [*Hildreth*, 1987; *Fierstein and Hildreth*, 1992; *Hildreth and Fierstein*, 2000; *Fierstein and Wilson*, 2005; *Hildreth and Fierstein*, 2012]. The initial ash flows were rhyolitic with subsequent eruptions having increasing proportions of andesitic and dacitic material [*Fierstein and Wilson*, 2005; *Hildreth and Fierstein*, 2012]. Fe-Ti oxide geothermometry indicates magmatic temperatures of 805–850°C for the rhyolite, increasing to 955–990°C for the andesitic eruptions [*Hildreth and Fierstein*, 2000], although recent work [e.g., *Lattard et al*., 2005] suggests that the method used may overestimate magmatic temperatures for the relatively high fO_2 conditions that are common for rhyolitic to andesitic material. The valley-filling outflow sheets reach a thickness of >170 m in the upper VTTS [*Kienle*, 1991]. Fumarole temperatures as high as 645°C were measured at ~3 km from the vent in 1919 [*Zies*, 1924], providing a minimum emplacement temperature for near-vent deposits. Samples collected in 2010 (Figure 1) from river-cut exposures include poorly to moderately welded ignimbrite, frequently with small (mm to cm-sized) pumice and lithic fragments distributed in the ash matrix. All samples were collected from the upper, more andesitic and dacitic sections, and the degrees of welding suggest emplacement at temperatures generally exceeding 550°C or 600°C [*Riehle*, 1973; *Sheridan and Ragan*, 1976; *Grunder et al*., 2005].

2.2. Mt. St. Helens 1980 Pyroclastic Eruptions

The 1980 eruptions of Mt. St. Helens were extremely well documented, with instrumentation and observers on the scene for the initial and largest event on 18 May, and for subsequent major pyroclastic eruptions on

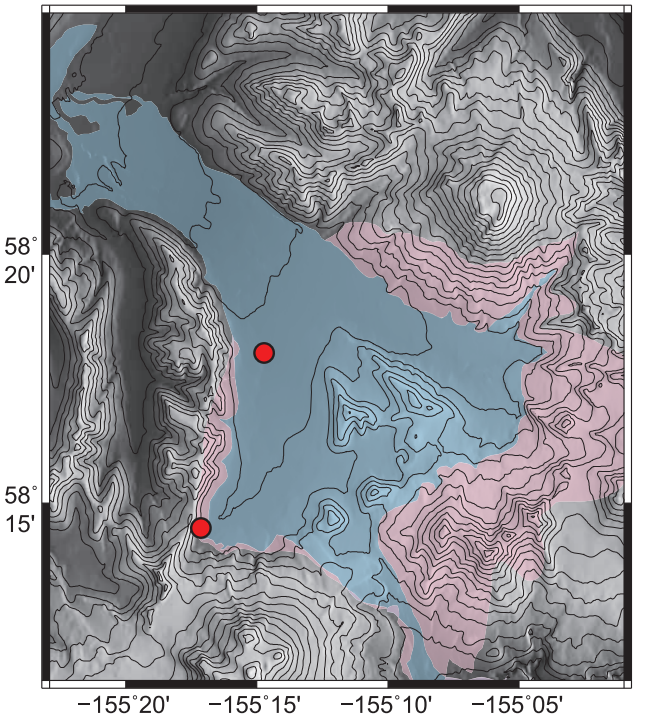

Figure 1. Novarupta 1912 eruption sampling locations (red circles). Pink shaded area denotes extent of the all rhyolite ignimbrite that formed the first phase of the eruption. Blue shaded area represents successive phases with increasing amounts of andesite and dacite. Sampling locations are all in the more andesitic and dacitic flows. Flow boundaries and vent location (heavy black line) from *Fierstein and Wilson* [2005].

25 May, 12 June, 22 July, 7 August, and 17 October [*Lipman and Mullineaux*, 1981]. The 18 May event began with the earthquake-triggered collapse of the inflated north flank of the volcano, in an enormous rockslide avalanche [*Christiansen and Peterson*, 1981; *Rosenbaum and Waitt*, 1981]. The rapid unloading triggered a series of northward-directed hydrothermal steam blasts, followed by a dacitic eruption which produced a Plinian ash column more than 20 km high and deposited voluminous pumiceous ash flows on the north slope. The subsequent eruptions were smaller in scale but each left significant deposits of nonwelded dacitic pumice and ash [*Christiansen and Peterson*, 1981].

Pre-eruptive magma temperature estimates range from 950°C to 1030°C [*Kuntz et al*., 1981; *Melson and Hopson*, 1981]. On eruption, the turbulent pyroclastic flows cooled in transit by entrainment of air and of previously deposited material eroded by the flows, especially on the higher portions of the north flank of the volcano. Farther downslope on the "pumice plain," deposition dominated over erosion, and flow units are typically a few meters in thickness [*Rowley et al*., 1981].

Temperature-depth, $T(z)$, profiles of the deposits were measured by thermocouple probes at numerous sites soon after emplacement of each of the flow units [*Banks and Hoblitt*, 1981], and repeated measurements over time intervals up to a few months allowed the construction of temperature-depth-time functions, $T(z,t)$, from which initial emplacement temperatures and in-situ thermal diffusivities could be determined [*Banks and Hoblitt*, 1981, 1996]. In general, emplacement temperatures (T_{empl}) were lowest for the initial 18 May deposits (100–325°C for the blast deposits, 300–420°C for the pyroclastic deposits), increasing for the later events: 361–602°C for 12 June; 642–688°C for 22 July; 645–850°C for 7 August; and 567–849°C for the second of two events on 17 October. Emplacement temperatures generally were highest near the eruptive source, decreasing by about 200°C over the first few hundred meters, and thereafter much more slowly with distance (at a rate on the order of 20°C km^{-1}) [*Banks and Hoblitt*, 1981, 1996].

Magnetic phases in the May–August pyroclastic pumice deposits were characterized soon after emplacement, by optical microscopy on polished grain mounts and by thermomagnetic analysis [*Kuntz et al*., 1981]. Two populations of oxides were recognized in the microscopic study: (a) titanomagnetites and titanohematites with grain sizes up to 250 μm, mostly homogeneous but with a few percent showing oxyexsolution, interpreted as primary minerals that crystallized in the magma chamber and rapidly cooled on eruption; and (b) titanomagnetites and titanohematites with complex intergrowth structures and altered margins, interpreted as xenolith fragments or xenocrysts. The homogeneous magmatic grains were the volumetrically dominant oxide phase in all of the pyroclastic flows after 18 May, with xenocrysts constituting only a few percent of the oxides in the 25 May, June, and August deposits and up to 10% in the July deposits. In the 18 May deposits, the basal layers were found to contain roughly equal amounts of primary magmatic and xenolithic oxides, and the proportion of the latter decreased to about 2% in the uppermost layers [*Kuntz et al*., 1981]. Thermomagnetic curves (saturation magnetization versus temperature) of magnetic

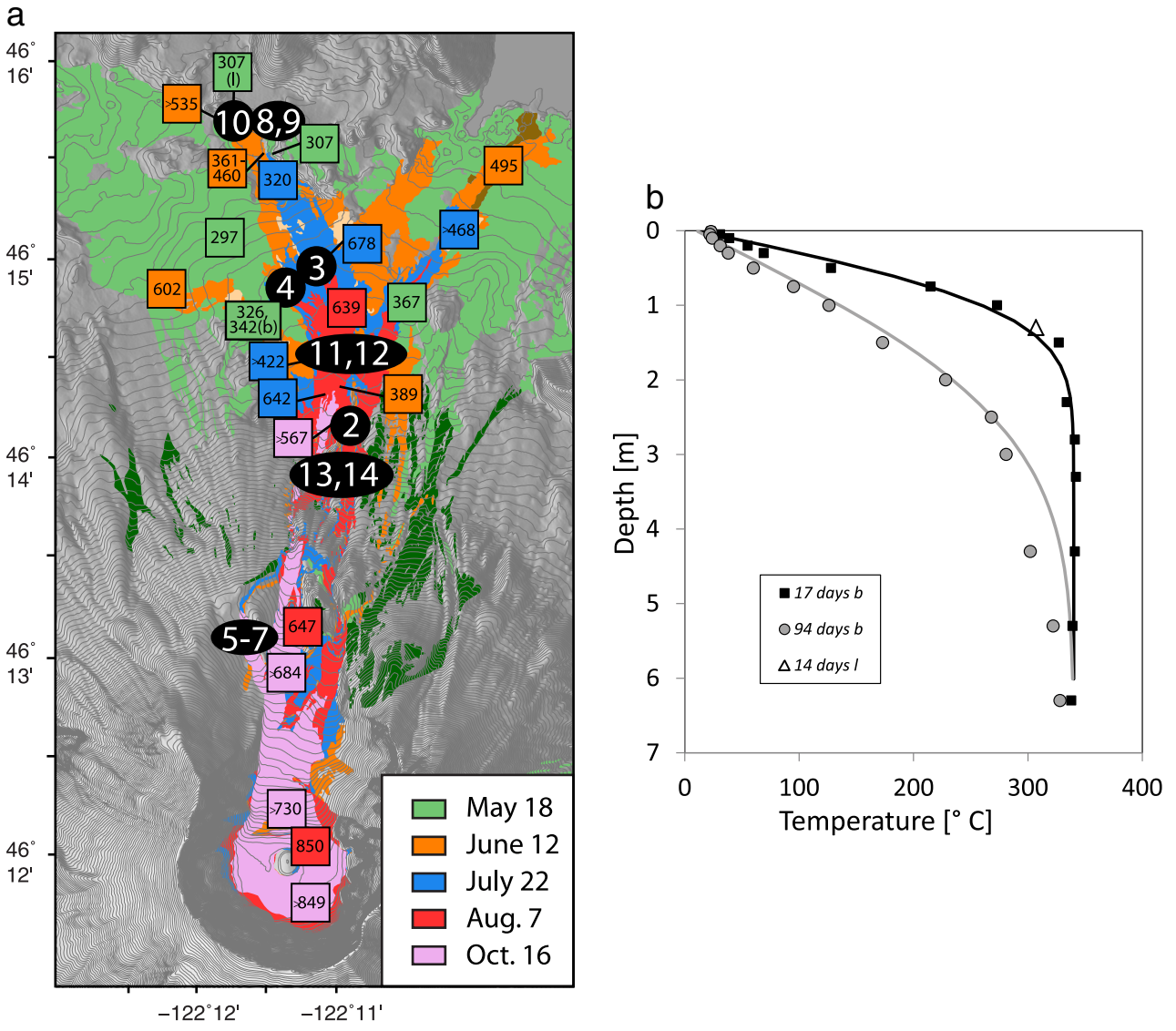

Figure 2. (a) Location of sites MSH002-MSH014 from the 2010 sampling of this study (numbers in black circles) on the northern flank of Mt. St. Helens. Also shown are pyroclastic flow units of the 1980 eruptive sequence [*Kuntz et al.*, 1990] and measured emplacement temperatures (corresponding colors) from *Banks and Hoblitt* [1996], including the locations of their stations b and l. (b) Temperature profiles: measured (symbols) [from *Banks and Hoblitt*, 1996] and calculated $T(z,t)$ (curves; assumed thermal diffusivity $= 2.5 \times 10^{-7}$ m/s^2) for stations b and l of *Banks and Hoblitt* [1996] in the May 18 pyroclastic deposits; locations are indicated in Figure 2a by temperatures of 342°C (T_{empl} for station b) and 307°C (single measurement for station l).

separates from pumice samples were found to be generally reversible, with a single dominant Curie temperature of about 370 ± 10°C in all of the flow units [*Kuntz et al.*, 1981].

Our 2010 sampling expedition focused on oriented samples of the 1980 pumice pyroclastics with broad areal coverage and a range of emplacement temperatures. A second, 2012 expedition focused on detailed (unoriented) stratigraphic coverage of one of the 18 May pyroclastic flows. Figure 2a shows our site locations together with flow-unit boundaries [*Kuntz et al.*, 1990] and emplacement temperatures [*Banks and Hoblitt*, 1996]. Where multiple flow units are superposed it was difficult to recognize their boundaries and to ascertain with certainty which units we sampled. Site MSH008, interpreted to be in the 18 May pyroclastic deposits, was resampled in 2012 as site MSH12-08. At this location, the upper flow surface was clearly marked by the distinctive overlying airfall ash deposits, and 21 levels were sampled below this surface, to a maximum depth of 158 cm. For most levels the sample contained one or more pumice blocks, typically a few cm in diameter, and 30–40 grams of ash matrix. Figure 2b shows a $T(z,t)$ data set of *Banks and Hoblitt* [1996] from their station *b*, approximately 2 km upslope from MSH12-08 (the nearest of their detailed

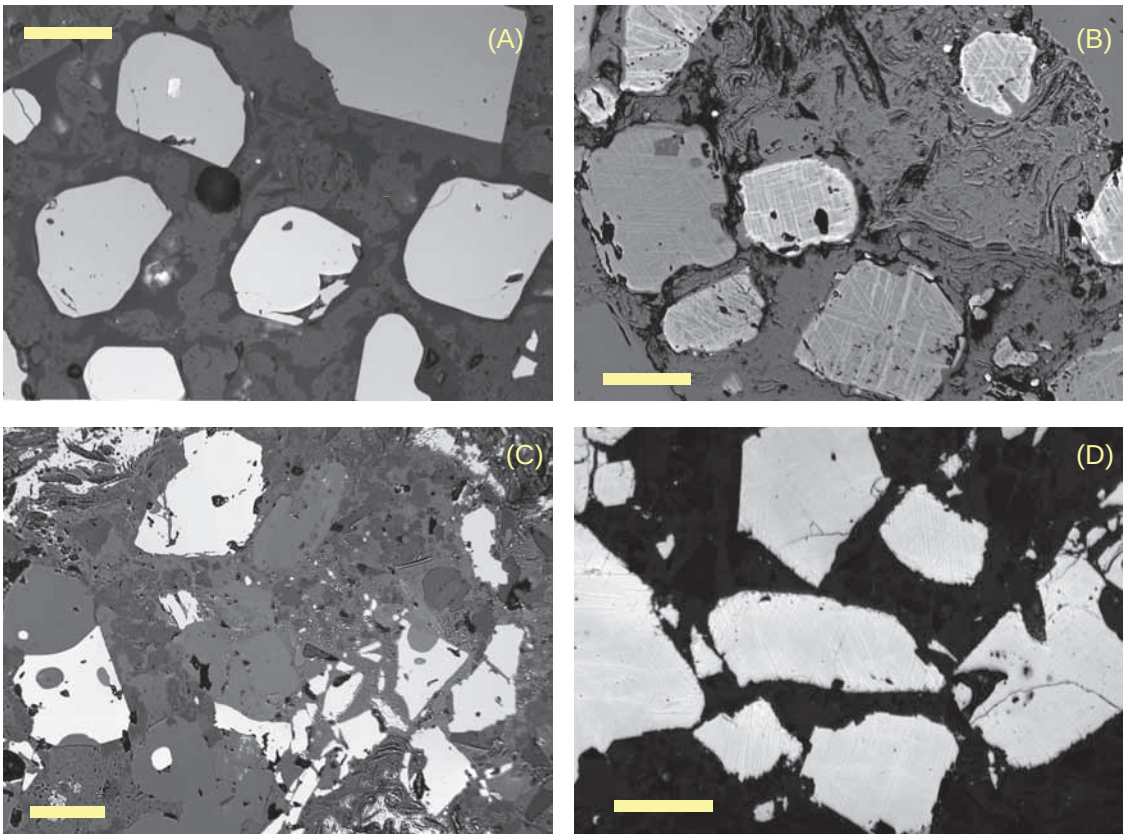

Figure 3. Reflected-light microscopic images of oxide grains magnetically extracted from (a and b) two Mt. St. Helens samples and (c and d) two Novarupta samples, pressed in phenolic resin and polished with diamond slurries and colloidal silica. MSH008-M ($T_{empl} \sim 340°C$; dominant $T_C \sim 377°C$; Figure 3a); oxides are optically homogeneous. MSH003-G ($T_{empl} \sim 650°C$; dominant $T_C \sim 529°C$; Figure 3b); almost all oxide grains exhibit oxyexsolution lamellae. NV039A (dominant $T_C \sim 400°C$; Figure 3c); oxides are optically homogeneous. NV037-Bx (dominant $T_C \sim 523°C$; Figure 3d); almost all oxide grains exhibit oxyexsolution lamellae. Scale bars are 50 μm for all images.

profiles in the 18 May pyroclastic deposits), for which they determined an emplacement temperature of 342°C. Also shown is their single measurement from station *l*, approximately 300 m from our site MSH12-08. Here the measured temperature of 307°C provides a minimum estimate of T_{empl} for our site MSH12-08; the similarity with the $T(z,t)$ function for station *b* of *Banks and Hoblitt* [1996] suggests emplacement at about 340°C.

3. Microscopic Observations and Microprobe Chemical Characterization

In order to maximize the number of magnetic crystals that could be analyzed, we used magnetic extracts from ash or from crushed pumice fragments, pressed in phenolic resin and polished with diamond slurries and colloidal silica. The extracts were examined in reflected light with a Leitz petrographic microscope. As previously reported by *Kuntz et al*. [1981] for the Mt. St. Helens samples, we find that the magnetic oxides in these pyroclastic deposits consist primarily of optically homogeneous titanomagnetites with typical sizes of 10–200 μm (Figures 3a and 3c). However we find significantly higher proportions of oxyexsolved grains in many sites (Figures 3b and 3d) than found by *Kuntz et al*. [1981], ranging up to nearly 100% in some samples. The exsolution textures are very similar to those associated with slow cooling and/or oxidizing conditions in other pyroclastic deposits [e.g., *Saito et al*., 2004; *Turner et al*., 2008], corresponding to oxidation classes C2 and C3 of *Haggerty* [1991]. Magnetic force microscopy (results not shown) confirms that (a) the optically homogeneous grains are magnetic and are homogeneous on scales down to tens of nanometers, and (b) the lamellae in the oxyexsolved grains are nonmagnetic or paramagnetic at room temperature. To the extent that we are able to relate the emplacement temperatures of *Banks and Hoblitt* [1996] to our site locations, there is a strong association between the proportions of oxyexsolved grains and T_{empl}, and there are also generally higher proportions of them in ash matrix than in pumice fragments within each site.

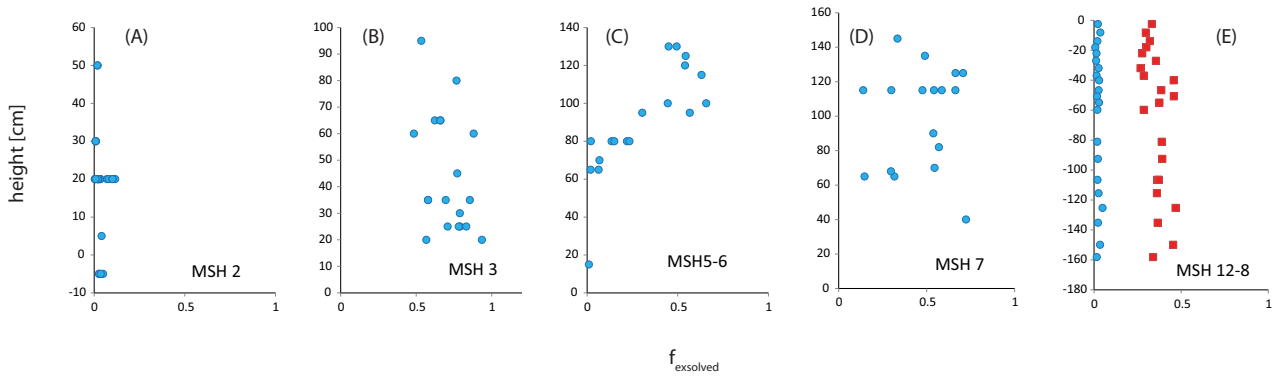

Figure 4. Proportion of susceptibility attributable to high-T_C oxyexsolved titanomagnetites for five stratigraphic sections in the Mt. St. Helens pyroclastic deposits (blue diamond = pumice, red square = ash). The fraction is calculated as $f_{exsolved} = [k(525°C) - k(600°C)]/[k_{max} - k(600°C)]$, where k_{max} typically occurs near 400°C, as in Figure 4. Sample position within each section is indicated by height above or below a reference level that was arbitrarily defined for the first four sections and that was defined by the upper surface of the flow for MSH12-8. Estimated emplacement temperatures based on data of *Banks and Hoblitt* [1996] and on site locations are as follows: (a) MSH002 (June) 361–602°C; (b) MSH003 (June or July) $\geq$ 600°C; (c and d) MSH005–007 (near vent, June, July, August, or October) $\geq$ 600°C; (e) MSH12-08 (May) $\sim$ 340°C.

Like most natural titanomagnetites, the homogeneous grains present in these rocks have moderate degrees of Mg and Al substitution and minor amounts of Mn. Average compositions are $Fe_{2.50}Ti_{0.30}Mg_{0.09}Al_{0.09}Mn_{0.01}O_4$ for Mt. St. Helens and $Fe_{2.57}Ti_{0.26}Mg_{0.06}Al_{0.08}Mn_{0.03}O_4$ for Novarupta (see *Bowles et al.* [2013], for ternary plot and table of sample-level results). This composition for the Mt. St. Helens titanomagnetites is very similar to that of *Melson and Hopson* [1981] for the 1980 eruptive sequence: $Fe_{2.47}Ti_{0.31}Mg_{0.08}Al_{0.11}Mn_{0.02}O_4$. The composition of these titanomagnetites overlaps data from most andesites, dacites, and rhyolites [*Ghiorso and Evans*, 2008], as well as some basalts [e.g., *Kawabata et al.*, 2011]. Most samples additionally contain a variable fraction of oxyexsolved titanomagnetites, as described above. Transects measured across exsolution lamellae in several exsolved crystals give average crystal compositions similar to that of the homogeneous grains, suggesting that the exsolved grains resulted from oxidation of the homogeneous grains.

4. Thermomagnetic Behavior and Irreversibility

In contrast to the findings of *Kuntz et al.* [1981], we observe a broad range of Curie temperatures in the 1980 Mt. St. Helens and the Novarupta pyroclastics, extending from about 370°C to above 550°C, and our thermomagnetic curves are very commonly irreversible, in a distinctive way. For many samples, multicycle thermomagnetic analyses using low-field AC susceptibility $k(T)$ or strong-field magnetization $M_S(T)$ initially show reversible behavior up to 400°C or above, with persistent high k or M_S in those heating/cooling cycles clearly indicating that T_C exceeds 400°C [see *Bowles et al.*, 2013, Figure 2]. Commonly one or occasionally two subsequent cycles to higher temperatures are irreversible in the 450°C–500°C range; the Curie temperature for the cooling leg (typically ~375°C, matching that found by *Kuntz et al.* [1981]) is significantly lower than that of the heating leg, but most often there is little or no change in the room temperature value of M_S or k [see *Bowles et al.*, 2013, Figure 2]. Continued heating/cooling cycles to still higher temperatures (maximum of 600°C–650°C) are reversible, with $T_C \sim$ 375°C. Many samples exhibit two-phase behavior, with a stable, higher-T_C (525°C–580°C) phase that does not change during the experiment, in addition to the lower-T_C phase whose Curie temperature is reduced by exposure to temperatures of 450°C or above. Comparison of thermomagnetic behavior and microscopic observations clearly indicates that the stable, higher-T_C (525°C–580°C) phase is oxyexsolved titanomagnetite, with Ti-rich lamellae in a Ti-depleted host, and that the lower-T_C phase associated with the irreversible behavior is optically homogeneous titanomagnetite. The reduced Curie temperatures at the end of the thermomagnetic experiments (approximately 375°C, with some intersite variation) agree with those reported by *Kuntz et al.* [1981] and are broadly compatible with the expected values for the measured compositions [e.g., *Creer and Stephenson*, 1972; *Richards et al.*, 1973; *Nishitani*, 1981; *Özdemir and O'Reilly*, 1982; *Hunt et al.*, 1995; *Lattard et al.*, 2006], as we will show in more detail in section 4.3.

4.1. Spatial Variation in Curie Temperature

The thermomagnetic behavior for our MSH samples corresponds in a general way with emplacement temperature, and more strongly with stratigraphic position within flow units. Curie temperatures of 550°C or above, associated with the oxyexsolved titanomagnetites, occur most prominently in sites with T_{empl}

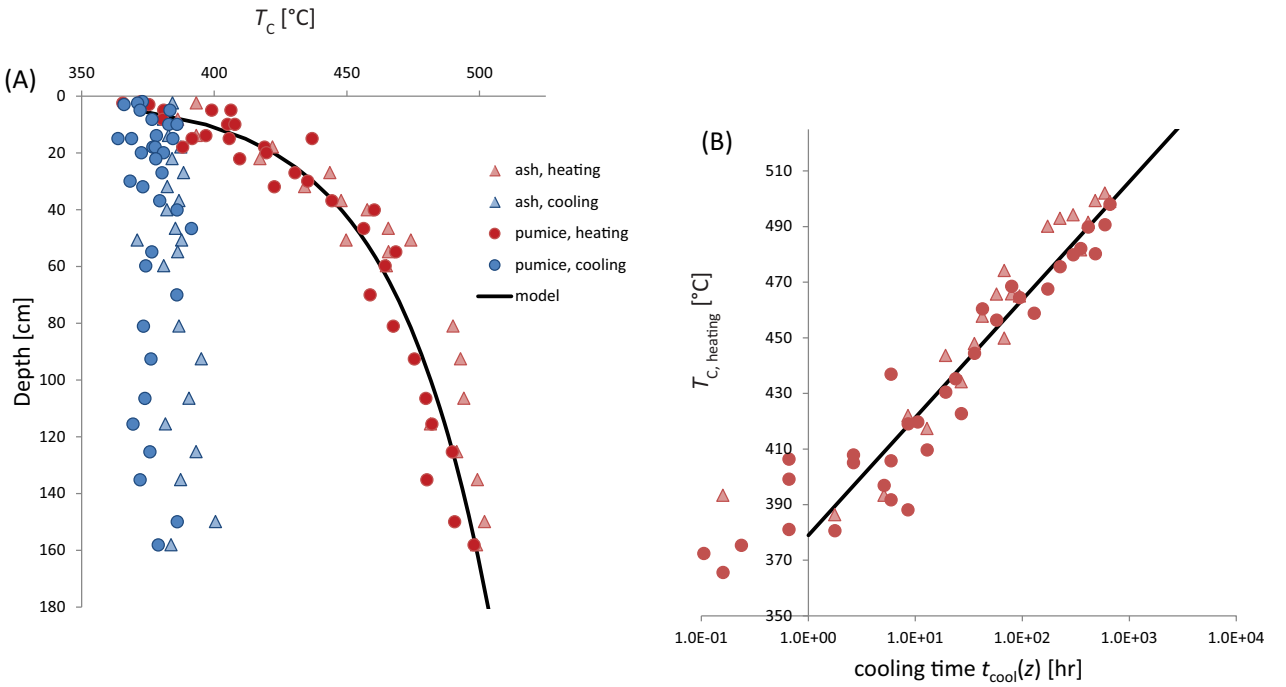

Figure 5. (a) Curie temperatures determined from the heating (red) and cooling (blue) legs of $k(T)$ thermomagnetic curves for samples collected over a range of depths within a single pyroclastic flow at site MSH12-8, showing depth-independent values of $T_{C,cooling}$ and a systematic increase in $T_{C,heating}$ with depth. Circles and triangles, respectively, indicate pumice and ash samples. (b) Heating-leg Curie temperatures scale with the logarithm of the depth-dependent cooling time, calculated from a one-dimensional conductive cooling model.

exceeding 600°C (sites which also commonly exhibited a pronounced reddish color, including MSH003, MSH006, MSH007, and MSH011), and the high-T_C phase is also generally more prominent in ashes than in pumices from the same site (Figure 4e). The high-T_C phase in the ash probably comes from both oxyexsolved magmatic titanomagnetites and fragments of foreign lithic material, which are "ubiquitous" in the ash [*Rowley et al*., 1981]. In most cases there is no systematic stratigraphic change in the relative proportions of the low-T_C and high-T_C phases, except in the section containing sites MSH005 and MSH006 (respectively below and above a height coordinate of 85 cm; Figure 4c; these sites were interpreted as representing different flow units). The Novarupta samples generally contain relatively high proportions of oxyexsolved grains, attributable to both comparatively high emplacement temperatures and small proportions of pumice. In cases where pumice fragments could be separated out, thermomagnetic analyses indicated a higher ratio of homogeneous ($T_C < 400$°C) to oxyexsolved ($T_C > 500$°C) titanomagnetites than in the bulk Novarupta samples.

For the homogeneous titanomagnetites, there does not appear to be any simple, direct relationship between T_C and T_{empl}. Initial $T_{C,heating}$ for this phase ranged from about 350°C to nearly 500°C in samples from almost all sites (the lone exception being site MSH002, where thermomagnetic curves were all reversible, and Curie temperatures of untreated samples did not exceed 370°C). In samples with very high proportions of oxyexsolved titanomagnetites ($f_{exsolved} > 0.75$), it was often impossible to define a precise T_C for the homogeneous phase, but the values generally appeared to be similar to those in the other samples ($T_{C,heating} \sim 400$°C–475°C; $T_{C,cooling} \sim 350$°C–375°C). There are slight inter-site differences in $T_{C,cooling}$ that are probably due to variations in the composition of the homogeneous titanomagnetites.

The clearest and most striking relationship between natural thermal history and laboratory thermomagnetic behavior is shown in the stratigraphic profile for MSH12-008. The initial Curie temperature measured during heating varies strongly and systematically as a function of depth within the flow unit, increasing from near-surface values of ~380°C all the way to 500°C at a depth of 150 cm (Figure 5a). In contrast, the final $T_{C,cooling}$ is essentially independent of depth (~380°C), as is the stable higher Curie temperature in the ash samples where it is present (~550°C, not shown). We note again that the thermomagnetic data of *Kuntz et al*. [1981] were all essentially reversible curves with $T_C \sim 375$°C. It is now clear that because their sampling was necessarily limited to the upper levels of each flow unit, the elevated Curie temperatures at depth were

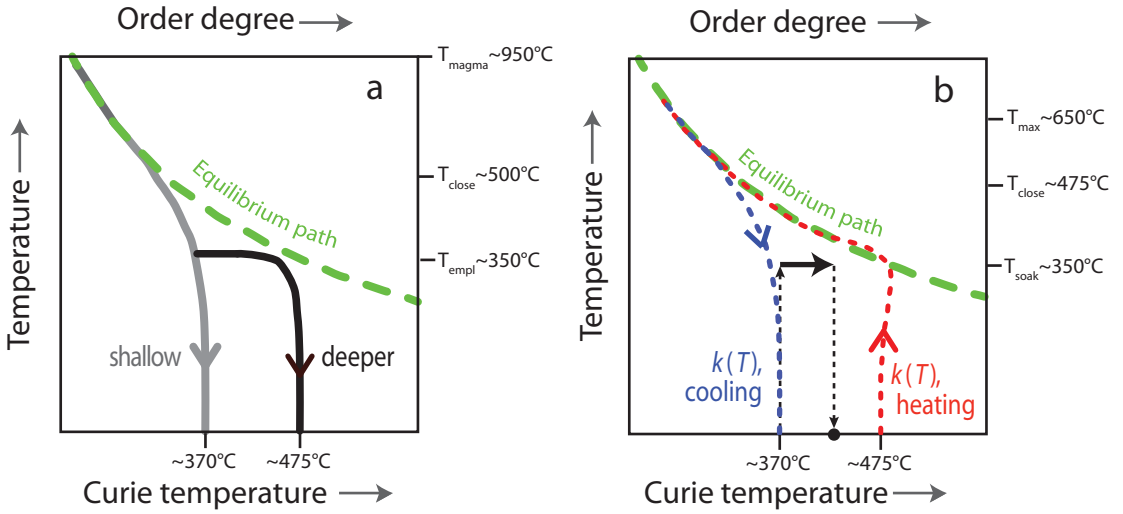

Figure 6. Schematic model of changes in cation ordering and in Curie temperature (a) during natural cooling and (b) during laboratory experiments, after *Harrison and Putnis* [1999a]. The spinel inversion parameter b increases from $^2/_3$ for a fully disordered (random) arrangement to 1 for a perfectly ordered inverse spinel, and more ordered cation distributions are expected to have higher Curie temperatures. The equilibrium distribution (dashed green) is more random at elevated temperature and more ordered at lower T. Redistribution of cations is also T-dependent, occurring rapidly at high temperature and more slowly at lower T. At the magmatic temperature T_{magma}, the cation distribution is highly disordered. On eruption and initial cooling, the distribution becomes more ordered, following the equilibrium path to the closure temperature T_{close}, where reordering rates become low enough to "freeze" the distribution (Figure 6a). Following emplacement, temperature remains constant at T_{empl} for an interval whose length increases with depth; during this time and during the subsequent resumption of slow cooling, the distribution evolves toward equilibrium, increasing the degree of order and T_C. Evolution of the cation distribution during thermomagnetic runs and isothermal annealing (Figure 6b) qualitatively explains the changes we observe in Curie temperature; red and blue paths, respectively, represent heating and cooling in a k(T) run, and black path represents isothermal annealing.

unobserved in their study. The lack of similar observed $T_C(z)$ trends at our other MSH and NV sites is explained by the fact that most of the variation in T_C occurs close to the flow surface. Sampling was not conducted with the specific goal of capturing near-surface trends, and, with the exception of MSH12-008, the upper parts of the flows have not been preserved or were not sampled.

This distinctive $T_C(z)$ pattern seems clearly to be a result of the post-emplacement thermal history, and is compatible with the cation-ordering mechanism proposed by *Bowles et al.* [2013]. At the high temperatures in the magma chamber before eruption, the cation distribution should be very disordered (Figure 6a). On initial rapid cooling during transport between eruption and emplacement, the distribution can be expected to evolve, following the equilibrium state as it becomes progressively more ordered. When the titanomagnetites cool to a closure temperature around 500°C, the cation distribution becomes "blocked" as the timescale of redistribution becomes long compared to the cooling timescale. The emplacement temperature may in general be higher or lower than the cation closure temperature, but here $T_{empl} \sim 350°C$, well below the closure temperature. In either case, post-emplacement cooling histories depend on depth within a flow: conductive cooling models predict a post-emplacement quasi-isothermal time interval whose duration increases with depth, during which the temperature ($T \sim T_{empl}$) remains essentially constant before cooling resumes; during this interval, the cation distribution evolves toward the equilibrium arrangement at T_{empl}, and after the subsequent resumption of slow cooling it continues evolving slowly toward higher order (Figure 6a).

We can model this thermal evolution by supposing that these pyroclastic flows were emplaced essentially isothermally ($T(z,0) = T_{empl}$) and that subsequent cooling took place mainly by conduction to the surface and to the cooler underlying rock; the data and calculations of *Banks and Hoblitt* [1996] are generally consistent with this. Under such conditions, the temperature profile evolves according to the half-space error-function cooling model [e.g., *Turcotte and Schubert*, 1982; *Wallace et al.*, 2003]:

$$\theta = \frac{T(z,t) - T_{empl}}{T_{surf} - T_{empl}} = \mathrm{erfc}\left(\frac{z}{2\sqrt{\kappa t}}\right) \quad (1)$$

where *erfc* is the complementary error function, T_{surf} is the surface boundary-value temperature (held constant), θ is the dimensionless temperature ratio, and κ is the thermal diffusivity. *Banks and Hoblitt* [1996]

found in situ diffusivities in the range 2.2×10^{-7} to 4.0×10^{-7} m^2/s; we used 2.5×10^{-7} to match their station b data in Figure 2b.

For specified values of T_{empl} and T_{surf} we can rearrange the above equation and solve for $t_{cool}(z)$, the depth-dependent time required to cool from T_{empl} to a specified temperature which we denote $T(z, t_{cool})$:

$$\theta_{cool} = \frac{T(z, t_{cool}) - T_{empl}}{T_{surf} - T_{empl}}$$
$$t_{cool}(z) = \frac{z^2}{4\kappa[\mathrm{erfc}^{-1}(\theta_{empl})]^2} = cz^2 \quad (2)$$

As we will show later, isothermal annealing experiments indicate that the increase in T_C with annealing time is much slower at 300°C than at 350°C or 400°C, so we set $T(z, t_{cool}) = 300$°C and use (2) to calculate the time required at each depth to cool to 300°C from an estimated emplacement temperature of 350°C, with a surface temperature of 10°C and a thermal diffusivity of 2.5×10^{-7} m^2/s. This cooling time ranges from less than 1 h for the shallowest sampled depths to more than 1000 h at depths greater than 200 cm (Figure 5b). It is clear that the measured heating-leg Curie temperatures scale very closely with the logarithm of $t_{cool}(z)$, i.e., the log of the time spent at elevated temperature ($T \geq 300$°C) after emplacement. This is the same functional dependence found by *Bowles et al*. [2013] for increases in $T_{C,heating}$ produced by isothermal annealing in the laboratory over times up to 1000 h, which we will revisit in detail below. The best-fit line in Figure 5b (which excludes the data from depths less than 5 cm, with cooling times less than one hour and with $T_{C,heating} \sim T_{C,cooling} \sim 375$°C) has a slope of $dT_{C,heating}/d\log(t_{cool}(z)) = 42.4$. The same relationship is shown by the solid curve in Figure 5a.

4.2. Isothermal Annealing Experiments

As documented by *Bowles et al*. [2013], the decrease in T_C observed during thermomagnetic experiments can be reversed by isothermal annealing at moderate temperatures (300°C–450°C) in the laboratory, a change that we attributed to progressive ordering of the cation distribution from an initially more random state. We expand upon those experiments here. Each sample is heated to the annealing temperature T_{soak} and held at that temperature, in air, for a chosen duration t_{soak}, after which it is removed from the furnace, cooling within a few minutes to room temperature. It is then placed in a high-temperature susceptibility instrument (Kappabridge KLY-2 with CS-2 furnace or MFK1-FA with CS-4 furnace) for $k(T)$ thermomagnetic measurements, usually a single-cycle run to a maximum temperature of 600°C or 650°C. Upon completion of the $k(T)$ run, T_C has been reset to the lower value characteristic of the disordered, "quenched" state, and the sample is returned to the annealing furnace for another treatment.

Heating for intervals as short as 0.3 h produces significant increases in $T_{C,heating}$ with accompanying thermomagnetic irreversibility, and longer soak times produce systematically larger effects (Figure 7) [*Bowles et al*., 2013, Figure 3]. For each sample in all of the experiments with $T_{soak} < 500$°C, the thermomagnetic cooling curves are virtually identical, and it is only the heating curves that exhibit systematic changes related to the annealing treatments (Figures 7a and 7b). For samples that contain both homogeneous and oxyexsolved titanomagnetites, the annealing treatments have only minimal effects on the latter: T_C remains nearly constant (in the 525°C–580°C range), but the proportion of total susceptibility due to the oxyexsolved grains increases slightly as the experiments progress, as a result of slow oxidation and unmixing during repeated heatings [see *Bowles et al*., 2013, Figure 3]. Oxidation is much faster in heat treatments at 650°C, resulting in irreversible transformation of the homogenous lower-T_C grains (Figure 7c). Optical microscopy of grains extracted and polished after the 46 h 650°C heat treatment shows that all of them contain lamellae, finer in scale and somewhat less organized than those in Figures 3b and 3d.

In almost all of our experimental results, the homogeneous titanomagnetites exhibit a single dominant "inflated" Curie temperature in the heating leg of the $k(T)$ curves (Figure 7a), indicating that the underlying process occurs uniformly throughout the volume of the titanomagnetites. In a few cases involving relatively high annealing temperatures (>400°C), two distinct Curie temperatures are observed in the $k(T)$ heating curves, one of which usually corresponds closely to the cooling-curve T_C (Figure 7b). This indicates that annealing in these cases affects only a fraction of the homogeneous titanomagnetite volume. There is no permanent change produced by these annealing treatments, and subsequent treatments at lower

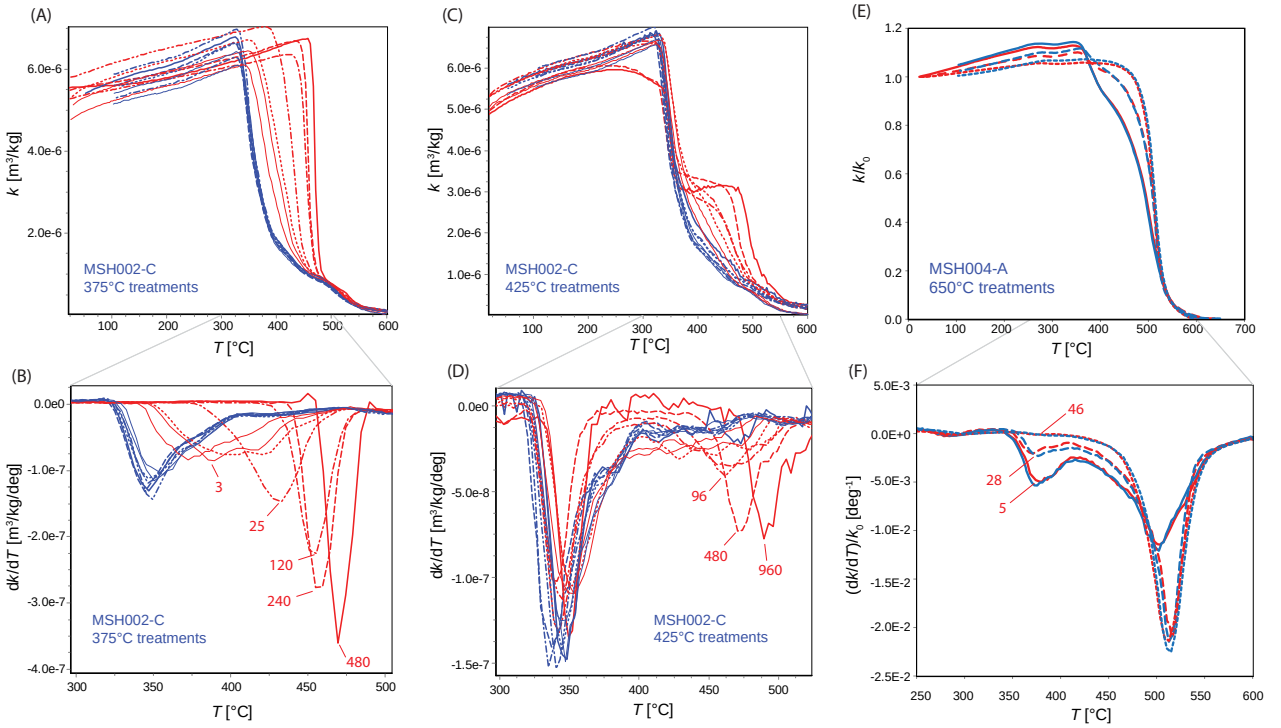

Figure 7. (a and b) ΔT_C produced by isothermal annealing in the laboratory at 375°C for varying durations, for a sample from Mt St Helens site MSH002. Derivative curves (Figure 7b) are labeled with anneal time in hours. Curie temperature observed for the heating leg (red) increases substantially and systematically with anneal time, whereas cooling-leg (blue) Curie temperature is independent of annealing treatment. Changes evidently occur uniformly throughout the volume of the homogeneous titanomagnetites in the sample; after each treatment there is a single dominant T_C for the heating leg. (c and d) Changes in T_C for the same sample during annealing at 425°C appear to occur heterogeneously within the volume of titanomagnetites in the sample; after each treatment there are two Curie temperatures for the heating leg, the higher of which is poorly defined for short soak times. (e and f) Oxyexsolution resulting from in-air annealing treatments at 650°C for varying durations, for a sample from Mt St Helens site MSH004, causes irreversible changes in the proportions of homogeneous ($T_C \sim 360$°C) and oxyexsolved ($T_C \sim 510$°C) titanomagnetites.

temperatures again uniformly affect the total volume of homogeneous titanomagnetite, resulting in a single dominant "inflated" Curie temperature.

In a few cases, we first measured low-temperature (20–300 K) susceptibility after an annealing treatment, then measured a high-temperature $k(T)$ curve, and then once again measured low-temperature susceptibility, in order to observe how the presumed relatively ordered and disordered cation distributions affect the low-T behavior. The low-temperature measurements were made on a Quantum Designs MPMS at frequencies between 1 and 1000 Hz; for clarity we show here (Figure 8) only the 1 Hz data. Generally the low-T susceptibility has a temperature dependence similar to those of synthetic titanomagnetites with x near 0.3 [*Moskowitz et al*., 1998; *Carter-Stiglitz et al*., 2006; *Engelmann et al*., 2010], with a very strong increase on warming, especially below about −120°C. In addition, a small but sharp drop just below 0°C indicates the presence of a phase in the hematite-ilmenite solid-solution series with a composition of $0.75 < y < 0.8$ (75–80% mole fraction of ilmenite) [*Lagroix et al*., 2004; *Burton et al*., 2008; *Engelmann et al*., 2010], and two stable (reversible) high-T_C phases are evident, a Ti-poor titanomagnetite (540°C) and nearly pure magnetite (580°C). Notably, there is no evidence for an ulvöspinel (−153°C) or other Ti-rich cubic phase T_C.

Significant changes in $k(T)$ are clearly produced in the low-T range as well as at high temperature (Figure 8). After annealing and before exposure to $T > 450$°C in the Kappabridge, susceptibility measured in the MPMS rises monotonically from $\sim$ −243°C to a peak near $\sim$ −20°C. Continued heating in the Kappabridge shows Curie points of 465°C on heating and 388°C during cooling from the maximum temperature. Low-T measurements in this disordered state show generally higher susceptibilities than in the initial run, and a nonmonotonic temperature dependence, with a clear peak near −120°C (Figure 8). The changes in $k(T)$ at low temperature, like those at high T, can be repeatedly produced by annealing and undone by cooling from temperatures above about 500°C.

As shown by *Bowles et al*. [2013], the increase in $T_{C,heating}$ is closely proportional to the logarithm of annealing time for treatments in the temperature range 300°C–425°C (Figure 9). The linear trends on the T_C-

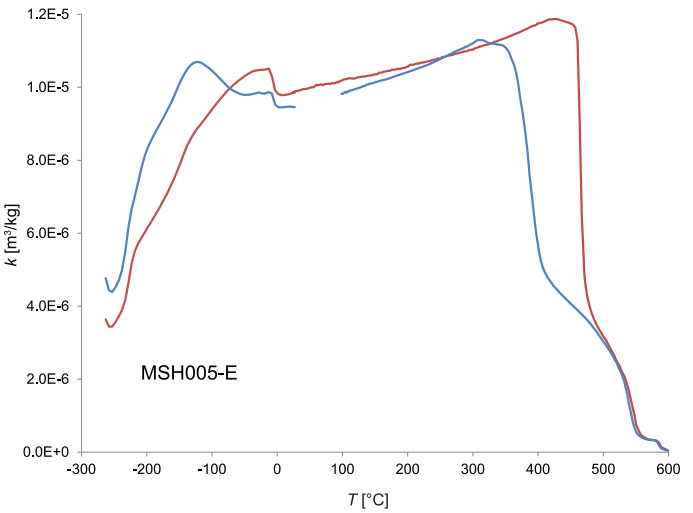

Figure 8. A sequence of $k(T)$ measurements made following a 475 h annealing at 350°C: first while warming from −253°C to 23°C in an MPMS at 1 Hz (red); then a heating (red) and cooling (blue) cycle to 600°C in a Kappabridge; and finally another low-T run in the MPMS (blue).

log(t_{soak}) plot are nearly parallel for the different treatment temperatures, and are generally shifted toward the left (shorter times) for higher temperatures. Annealing at temperatures >425°C (450°C and 500°C) produced little or no change in T_C, and as noted above, treatments in air at still higher temperatures (≥600°C) resulted in rapid irreversible oxyexsolution of the homogeneous titanomagnetites. Within the 300°C–425°C treatment range, there is little indication that the Curie temperature is reaching a plateau even after 1000 h, suggesting that the cation distributions are still evolving toward equilibrium states of greater order, and that kinetics in this temperature range are too sluggish for full equilibration to occur within these annealing times. For most samples the slope dT_C/dlog(t_{soak}) is between 20° and 30° per log-hour at temperatures between 300 and 425°C, and slopes are slightly higher on average for the Mt. St. Helens samples than for those from Novarupta.

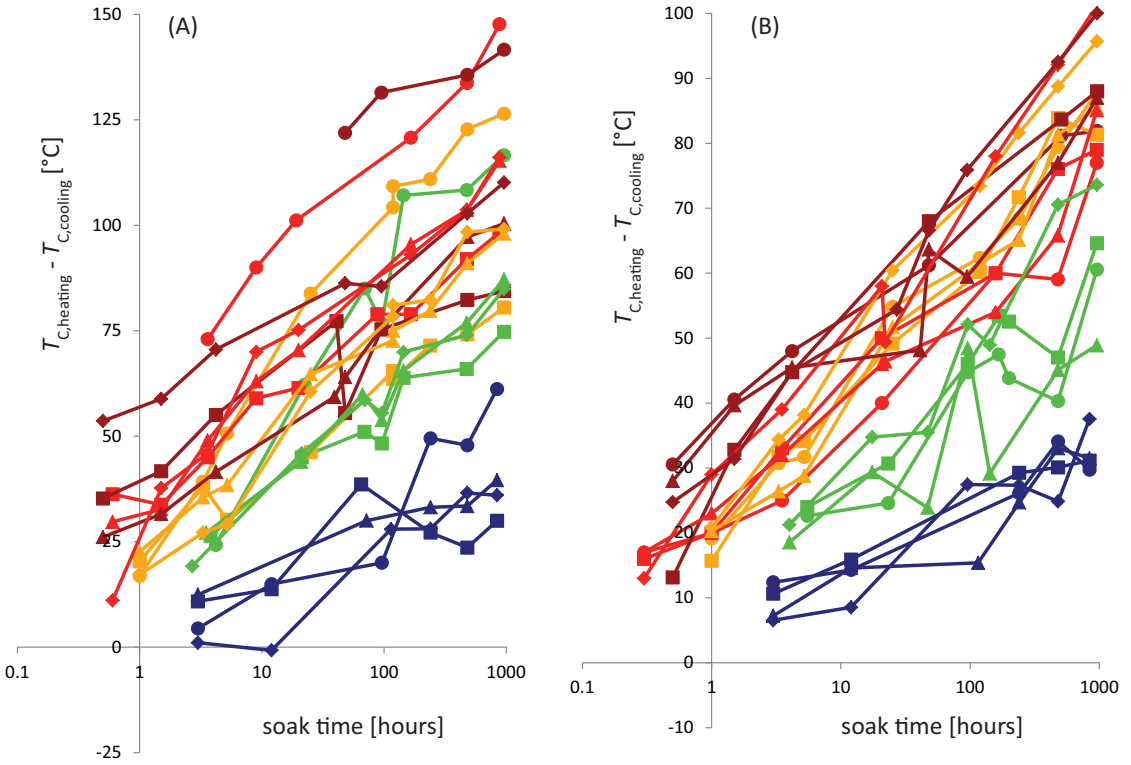

Figure 9. ΔT_C produced by isothermal annealing in the laboratory, for (a) Mt St Helens sites MSH002 (circles), MSH004 (squares), MSH005 (triangles), and MSH008 (diamonds), and (b) Novarupta sites NV013 (circles), NV014 (squares), NV017 (triangles), and NV039 (diamonds); blue, green, orange, red, and dark red indicate respective annealing temperatures of 300°C, 350°C, 375°C, 400°C, and 425°C. Note difference in vertical scales for the two plots.

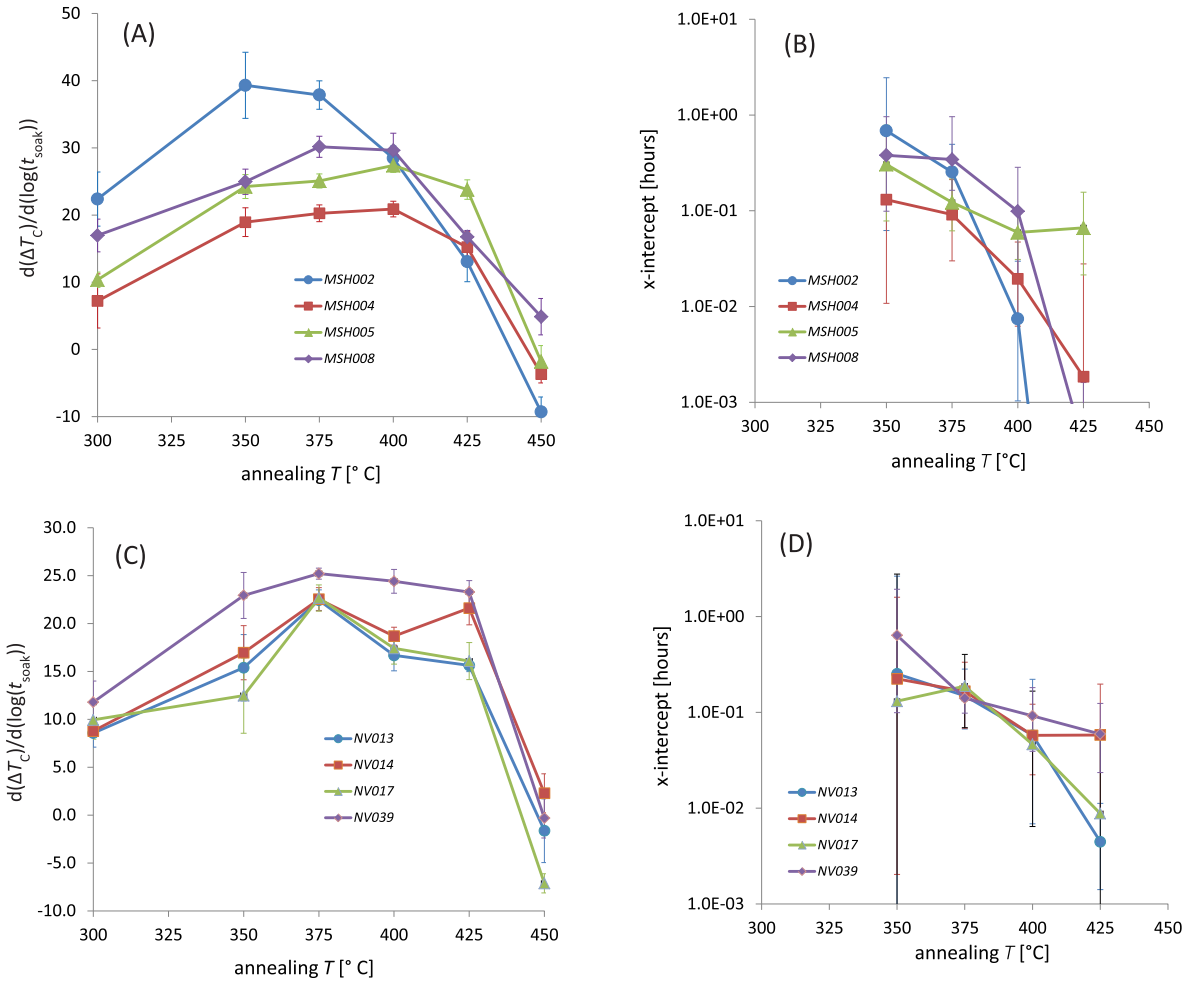

Figure 10. (a and c) Slopes and (b and d) horizontal-axis intercepts of least squares best fit lines to the ΔT_C (log(t)) data of Figure 9 for samples from Mt. St. Helens (Figures 10a and 10b) andNovarupta (Figures 10c and 10d). Intercepts were poorly defined for 300°C and 450°C because of the shallow slopes, and values are not shown.

Because of the somewhat noisy details and the overlap between data sets (Figure 9), the trends in $\Delta T_C(T_{soak}, t_{soak})$ can be seen more clearly when plotted as slopes and intercepts of the least-squares linear fits to $\Delta T_C(\log(t_{soak}))$, as in Figure 10. Such linear fits provide reasonable approximations of the $\Delta T_C(T_{soak}, t_{soak})$ behavior only over the range of soak times that we have explored in these experiments, and we expect that a larger time window would show the form of the function to be sigmoidal, with a lower limiting value of $\Delta T_C = 0$ for shorter timescales, and an unknown upper limiting value for sufficiently long times, representing an equilibrium state which is presumably temperature-dependent. The linear fit parameters in Figure 10 nevertheless contain important information on the kinetics of the mechanism underlying the changes in Curie temperature during the annealing experiments. The tendency noted above for the $\Delta T_C(\log(t_{soak}))$ trends to shift leftward with increasing T_{soak} is shown more clearly in the time-axis intercept plots, which indicate that a given change in T_C is produced 10–100 times faster at 425°C than at 350°C. The slopes $d\Delta T_C/d(\log(t_{soak}))$ vary nonmonotonically with T_{soak}, having maxima near 350°C–375°C. Lower slopes above 375°C and below 350° can be interpreted in terms of two temperature-dependent controlling factors (described more fully in the Discussion section below): the equilibrium cation distribution and its corresponding Curie temperature; and the cation diffusion or redistribution rates.

4.3. Compositional Controls on $T_C(T_{soak}, t_{soak})$

The cooling-leg Curie temperature for each specimen is observed to be essentially independent of experimental thermal history, and inter-sample variations in this property are most likely due to differences in composition of the titanomagnetites. Measured compositions [*Bowles et al.*, 2013] show significant

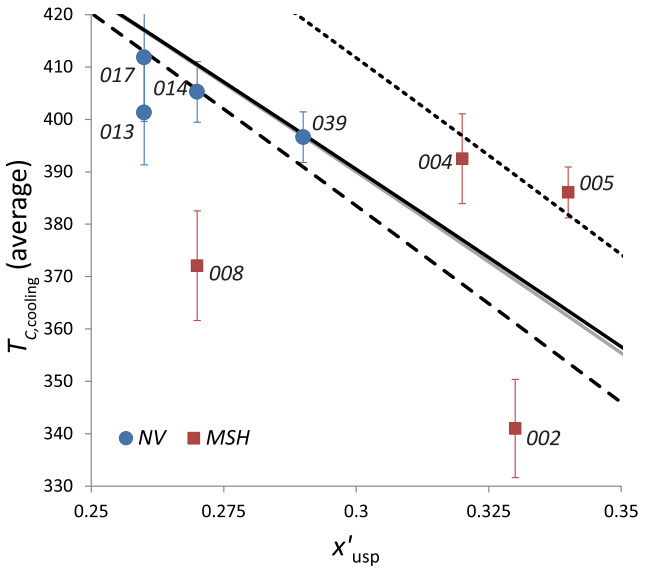

Figure 11. $T_{C,cooling}$ is determined primarily by the concentration of Ti, Al, and Mg in the titanomagnetites. x'_{usp} is the ulvöspinel compositional parameter calculated as projected onto the magnetite-ulvöspinel join [*Bowles et al*., 2013]. Solid curves are $T_C(x)$ fits from *Hunt et al*. [1995] (black) and from *Bleil and Petersen* [1982] (gray); dotted and dashed curves are, respectively, polynoms 1 and 3 of *Lattard et al*. [2006], for titanomagnetites synthesized in equilibrium with ilmenite (dotted) or with ulvöspinel (dashed). Red squares indicate samples from Mt. St. Helens; blue circles are for Novarupta; numbers indicate site number.

variability in the concentrations of Ti, Al, and Mg, and $T_{C,cooling}$ spans a range of about 75°C, from 340°C to 415°C. It is therefore of interest to examine the possible effects of composition on the ordering dynamics that are inferred to be responsible for changing Curie temperatures in these samples. Each point in Figure 11 represents a sample for which titanomagnetite composition was determined by microprobe measurements. For each sample, the average $T_{C,cooling}$ was calculated for all completed $k(T)$ runs (approximately 40 measurements of $T_{C,cooling}$). There is clearly, and unsurprisingly, a general negative correlation between Curie temperature and concentration of Fe-substituting cations (Table 1). The cooling-leg Curie temperatures correspond reasonably well with published titanomagnetite $T_C(x)$ compilations (Figure 11) when plotted as a function of an ulvöspinel compositional parameter x' projected onto the magnetite-ulvöspinel join ($x' = \mathrm{Ti}/(\mathrm{Ti} + \mathrm{Fe}^{3+}/2)$ [*Evans et al*., 2006]). Some scatter about this trend is expected due to varying proportions and differing effects of substituted Ti^{4+}, Al^{3+}, and Mg^{2+}. The largest deviations are for the two sites (MSH002 and MSH008) having the lowest proportions of oxyexsolved titanomagnetites.

The changes in T_C depend on time, temperature, and composition. An overall picture is obtained by plotting the slopes and intercepts of the $\Delta T_C(\log(t_{soak}))$ trends against the average $T_{C,cooling}$ for each specimen (Figure 12). $T_{C,cooling}$ serves as a proxy for titanomagnetite composition and allows us to include data for additional samples for which microprobe data are not available. The time-axis intercepts can be considered to represent a sort of threshold or activation time constant (at each soak temperature) for T_C changes; for shorter times $\Delta T_C = 0$, and above this threshold the slopes indicate the changes in T_C with each tenfold increase in annealing time.

The time-axis intercepts generally decrease systematically with increasing T_{soak}, as previously noted, and do not appear to exhibit any systematic changes with composition (Figure 12b and Table 2), except perhaps at

Table 1. Compositions and Cooling-Leg Curie Temperatures[a]

Sample	IGSN	Avg T_C Cooling	SD T_C Cooling	Al	Ti	Mg	Fe^{2+}	Fe^{3+}	Mn	x'
KM013-A	IRMP00GLI	401.3	10.0	0.09	0.25	0.07	1.15	1.41	0.02	0.26
KM014-B	IRMP00GLM	405.3	5.8	0.08	0.26	0.06	1.17	1.41	0.03	0.27
KM017-A	IRMP00GDK	411.8	12.2	0.1	0.25	0.06	1.16	1.4	0.03	0.26
KM039-A	IRMP00GDL	396.6	4.8	0.05	0.28	0.05	1.21	1.38	0.03	0.29
MSH002-G	IRMP00GVT	341.0	9.4	0.12	0.31	0.12	1.18	1.26	0.01	0.33
MSH004-A	IRMP00GI3	392.5	8.6	0.09	0.31	0.09	1.21	1.29	0.01	0.32
MSH005-E	IRMP00GWQ	386.1	4.9	0.06	0.33	0.07	1.25	1.28	0.01	0.34
MSG008-J	IRMP00GLE	372.1	10.5	0.08	0.26	0.1	1.15	1.4	0.01	0.27
MSH010-C	IRMP00GPS	365.2	4.5							
MSH011-F	IRMP00GTW	357.5	2.6							
MSH012-B	IRMP00GMB	366.8	3.4							
MSH12-09-A	IRMP00LV7	386.2	5.1							

[a]Averages and standard deviations calculated for all $k(T)$ experiments on each sample (approximately 40 measured values). Microprobe chemical compositions from *Bowles et al*. [2013].

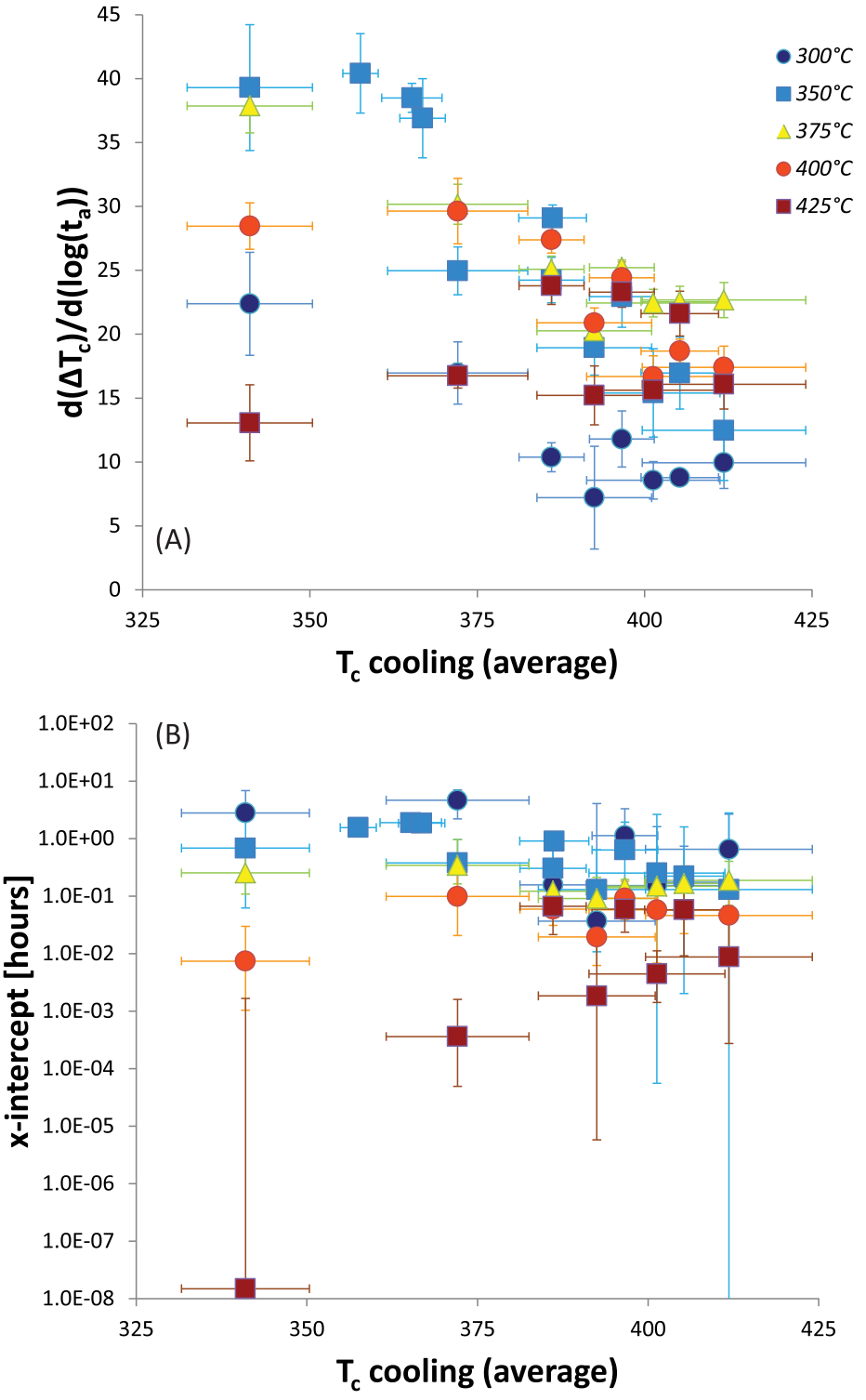

Figure 12. (a) Slopes and (b) time-axis intercepts of least squares best fit lines to the ΔT_C (log(t)) data of Figure 10, as functions of titanomagnetite composition (as indicated by $T_{C,cooling}$). From left to right (increasingly pure magnetite), the samples are from sites MSH002, MSH011*, MSH010*, MSH012*, MSH008, MSH005, MSH12-09*, MSH004, NV039, NV013, NV014, and NV017 (asterisks denote samples with annealing data for 350°C only).

the highest effective annealing temperature, 425°C. The very short timescale ($\sim 10^{-8}$ h) obtained for MSH002 at 425°C also has a large uncertainty due to heterogeneous reordering at that temperature (Figure 7b) and poor definition of T_C for short anneal times, resulting in a more limited data set for the linear fitting

Table 2. Rates of Change in Curie Temperatures During Experimental Annealing[a]

T_a	Fit Parameters	KM013 A	KM014 B	KM017 A	KM039 A	MSH00 2G	MSH00 4A	MSH00 5E	MSH00 8J	MSH01 0C	MSH01 1F	MSH01 2B	MSH12 09-A
300	$d(\Delta T_C)/d(\log(t_a))$	8.57	8.78	9.95	11.80	22.38	7.21	10.37	16.96				
300	R^2	0.92	0.99	0.86	0.88	0.86	0.54	0.80	0.79				
300	slope SD err	1.46	0.56	2.01	2.20	4.03	4.02	1.13	2.43				
350	$d(\Delta T_C)/d(\log(t_a))$	15.40	16.96	12.48	22.94	39.30	18.94	24.24	24.96	38.49	40.41	36.90	29.09
350	R^2	0.80	0.88	0.67	0.95	0.93	0.94	0.97	0.97	1.00	0.98	0.97	1.00
350	slope SD err	3.46	2.83	3.93	2.40	4.92	2.14	1.78	1.88	1.13	3.11	3.10	1.01
350	x_0	2.53E-1	2.24E-1	1.31E-1	6.38E-1	6.85E-1	1.31E-1	3.05E-1	3.80E-1	1.89E+0	1.56E+0	1.86E+0	9.08E-1
350	$(\Delta x_0)_{95}^-$	2.53E-1	2.22E-1	1.31E-1	5.39E-1	6.23E-1	1.20E-1	2.27E-1	2.81E-1				
350	$(\Delta x_0)_{95}^+$	2.39E+0	1.37E+0	2.65E+0	1.29E+0	1.77E+0	5.11E-1	4.79E-1	5.80E-1				
375	$d(\Delta T_C)/d(\log(t_a))$	22.44	22.54	22.67	25.22	37.86	20.26	25.08	30.16				
375	R^2	0.99	0.88	0.98	1.00	0.98	0.97	0.99	0.98				
375	Slope std err	1.08	1.21	1.37	0.57	2.12	1.25	1.04	1.56				
375	x_0	1.49E-1	1.66E-1	1.88E-1	1.41E-1	2.54E-1	9.12E-2	1.22E-1	3.43E-1				
375	$(\Delta x_0)_{95}^-$	8.20E-2	9.78E-2	1.19E-1	4.24E-2	1.45E-1	6.12E-2	6.05E-2	1.80E-1				
375	$(\Delta x_0)_{95}^+$	1.34E-1	1.67E-1	2.15E-1	5.38E-2	2.40E-1	1.21E-1	9.35E-2	6.17E-1				
400	$d(\Delta T_C)/d(\log(t_a))$	16.68	18.69	17.41	24.41	28.46	20.88	27.39	29.63				
400	R^2	0.95	0.99	0.95	0.98	0.98	0.98	0.99	0.96				
400	Slope std err	1.62	0.93	1.65	1.24	1.81	1.16	1.04	2.56				
400	x_0	5.77E-2	5.75E-2	4.64E-2	9.20E-2	7.42E-3	1.95E-2	5.94E-2	9.87E-2				
400	$(\Delta x_0)_{95}^-$	5.09E-2	3.52E-2	3.99E-2	5.28E-2	6.38E-3	1.32E-2	2.84E-2	7.79E-2				
400	$(\Delta x_0)_{95}^+$	1.64E-1	6.45E-2	1.21E-1	8.98E-2	2.24E-2	2.77E-2	4.33E-2	1.85E-1				
425	$d(\Delta T_C)/d(\log(t_a))$	15.63	21.61	16.08	23.29	13.06	15.22	23.79	16.75				
425	R^2	0.99	0.97	0.92	0.98	0.91	0.88	0.98	0.98				
425	Slope std err	0.65	1.75	1.94	1.19	2.98	2.31	1.46	0.97				
425	x_0	4.46E-3	5.81E-2	8.80E-3	5.95E-2	1.50E-8	1.85E-3	6.64E-2	3.63E-4				
425	$(\Delta x_0)_{95}^-$	3.05E-3	4.89E-2	8.53E-3	3.60E-2	1.50E-8	1.84E-3	4.50E-2	3.13E-4				
425	$(\Delta x_0)_{95}^+$	6.78E-3	1.39E-1	5.25E-2	6.46E-2	1.66E-3	2.60E-2	9.01E-2	1.25E-3				
450	$d(\Delta T_C)/d(\log(t_a))$	−1.62	2.29	−7.12	−0.31	−9.31	−3.66	−1.82	4.87				
450	R^2	0.11	0.39	0.96	0.01	0.90	0.79	0.16	0.62				
450	Slope std err	3.32	2.04	1.00	2.08	2.24	1.32	2.39	2.71				

[a]Fit parameters for linear regression of $\Delta T_C(\log(t_a))$ data of Figure 9. x_0 is the x axis (log-time axis) intercept and the $(\Delta x_0)_{95}$ values are the positive and negative error bounds for the intercept value at 95% confidence.

(Figure 9). On average there is a weak tendency for the time intercepts to increase with increasing cation substitution (decreasing $T_{C,cooling}$) for annealing temperatures of 300–375°C, and to remain flat or decrease slightly for $T_{soak} \geq 400$°C.

The slopes, in contrast, change strongly with both composition and temperature, becoming systematically larger in the more Ti-, Al-, and Mg-rich titanomagnetites, especially for annealing temperatures of 350°C–375°C (Figure 12a and Table 2). Calculated slopes range up to around 40°C per log unit, and maximum values are comparable to that inferred for the T_C enhancement during natural slow cooling after emplacement (Figure 5); such high slopes occur in the annealing experiments only for samples with $T_{C,cooling} < 370$°C.

5. Discussion

The results of the annealing experiments have implications for the mechanism responsible for the changes in T_C, and also for the interpretation of Curie temperatures found in the natural rocks. We will briefly discuss the links between oxidation-exsolution, emplacement temperature and cooling times before focusing on the dramatic T_C variations found in the homogenous titanomagnetite grains.

5.1. Oxyexsolution

Oxidation exsolution (oxyexsolution) of titanomagnetites irreversibly increases T_C [e.g., *Lattard et al.*, 2012] by transforming a single-phase cubic oxide into intergrowths of an Fe-rich cubic end-member (with a higher T_c) and a Ti-rich rhombohedral end-member (typically paramagnetic at room temperature). In our samples it occurs very slowly in the 300°C–425°C annealing experiments, gradually transforming the single-phase titanomagnetites. Cumulative heating times approaching 9000 h in this moderate temperature range have an effect comparable to that of a single 5 h treatment at 650°C (Figure 7c). High degrees of oxyexsolution (as observed to occur naturally in site MSH003) typically require heating in air for several hours at 600°C–700°C or for a few seconds at 1000°C–1300°C [*Lattard et al.*, 2012].

It is conceivable that the variations in $f_{exsolved}$ between sites (Figure 4) are related to different posteruptive thermochemical histories, especially involving different emplacement temperatures. However previous studies [*Saito et al*., 2004; *Turner et al*., 2008] have linked the proportion of oxyexsolved grains in pyroclastic deposits to different magmatic conditions prior to eruption. Slow magma ascent commonly results in formation of lava domes, in which oxygen fugacities may be locally high enough for relatively rapid oxidation and unmixing [*Saito et al*., 2004; *Turner et al*., 2008]. Dome collapse typically generates "block-and-ash" ignimbrite flows, and the 12 June deposits on Mt. St. Helens are described in this way [*Christiansen and Peterson*, 1981; *Moore et al*., 1981; *Olhoeft et al*., 1981]. This may account for the higher degrees of oxidation we find in MSH sites 003, 007, and 011. On the other hand, *Kuntz et al*. [1981] found low percentages of oxyexsolved titanomagnetite grains in pumices from all of the 1980 flow units. One way to reconcile our observations with those of *Kuntz et al*. [1981] is to postulate that significant oxyexsolution occurred in the high-T_{empl} deposits after emplacement, except in the most rapidly cooled surface samples which were accessible for collection and analysis soon after each eruption. Alternatively, one could imagine that $f_{exsolved}$ varies by location within some flow units as a consequence of spatial variations in oxidizing conditions within a lava dome prior to eruption. Other factors including gas permeability are also likely to play a significant role [e.g., *Tait et al*., 1998].

An interesting form of moderate-temperature oxidation in volcanic titanomagnetites has recently been documented by *Tanaka and Yamamoto* [2014]. Their reflected-light and electron microscopic observations as a function of thermal demagnetization temperature showed both a change in color and the emergence of submicron-scale "stripes" after treatments in the 300°C–400°C range, coinciding with the onset of nonideal Thellier-Thellier paleointensity behavior, and often coinciding with irreversible increases in T_C in stepwise thermomagnetic runs. Despite the correspondence with the temperature range over which we observe the strongest changes in T_C for our samples (Figure 10), it is clear that there are two distinct phenomena involved: moderate-temperature oxidation [*Tanaka and Yamamoto*, 2014] cannot account for the decreases in Curie temperature that we observe during $k(T)$ experiments.

5.2. Mechanism of Thermomagnetic Irreversibility in Homogeneous Titanomagnetites

Bowles et al. [2013] considered two possible temperature-dependent mechanisms for the observed changes in T_C in the homogeneous titanomagnetites: subsolvus unmixing/rehomogenization (into two cubic phases) and cation ordering/disordering. For the binary magnetite-ulvöspinel system, the full range of compositions $0 \leq x \leq 1$ is thermodynamically stable at sufficiently high temperatures; intermediate compositions become unstable at lower temperatures, where unmixing is favored but limited by temperature-dependent kinetics. Chemical unmixing may occur either by nucleation and growth of cubic-phase lamellae having near end-member composition, or by spinodal decomposition, in which short-wavelength low-amplitude compositional fluctuations develop and grow with time [e.g., *Harrison and Putnis*, 1999a]. The exact position and shape of the binary solvus are imperfectly known, but its crest is generally considered to be near 775 K for $x \sim 0.55$ [*Lindsley*, 1981; *Price*, 1981a; *Trestman-Matts et al*., 1983; *Lilova et al*., 2012]. Many of the significant changes that we observe in our annealing experiments occur near or below the binary solvus temperatures (Figure 13), suggesting that the observed increases in T_C may be related to unmixing of the homogeneous titanomagnetite into Ti-enriched and Ti-depleted regions, the latter having higher T_C than the homogeneous composition. This explanation then requires rapid rehomogenization (within minutes) at temperatures above about 450°C to account for the observed thermomagnetic irreversibility.

New annealing experiments (results not shown) have failed to produce any significant changes in T_C for the lower-x titanomagnetites in pyroclastic deposits from the Tiva Canyon Tuff ($x \sim 0.1$) [*Schlinger et al*., 1991; *Rosenbaum*, 1993; *Worm and Jackson*, 1999] and the Bishop Tuff ($x \sim 0.05$) [*Palmer et al*., 1996; *Gee et al*., 2010]. These compositions are far above the solvus at the experimental annealing temperatures, and the lack of observable changes in T_C in these samples thus appears to be consistent with the idea that subsolvus unmixing may play a role in the observed changes in the higher-x titanomagnetites of Novarupta and Mt. St. Helens.

The alternative model, preferred by *Bowles et al* [2013] for reasons to be discussed below, involves time and temperature-dependent redistribution of cations between and perhaps within the *A* and *B* sublattices of the titanomagnetites. Ferrous-ferric exchange between sublattices in titanomagnetite is considered to be fast even at room temperature [e.g., *Jensen and Shive*, 1973; *Wechsler et al*., 1984], involving only the transfer

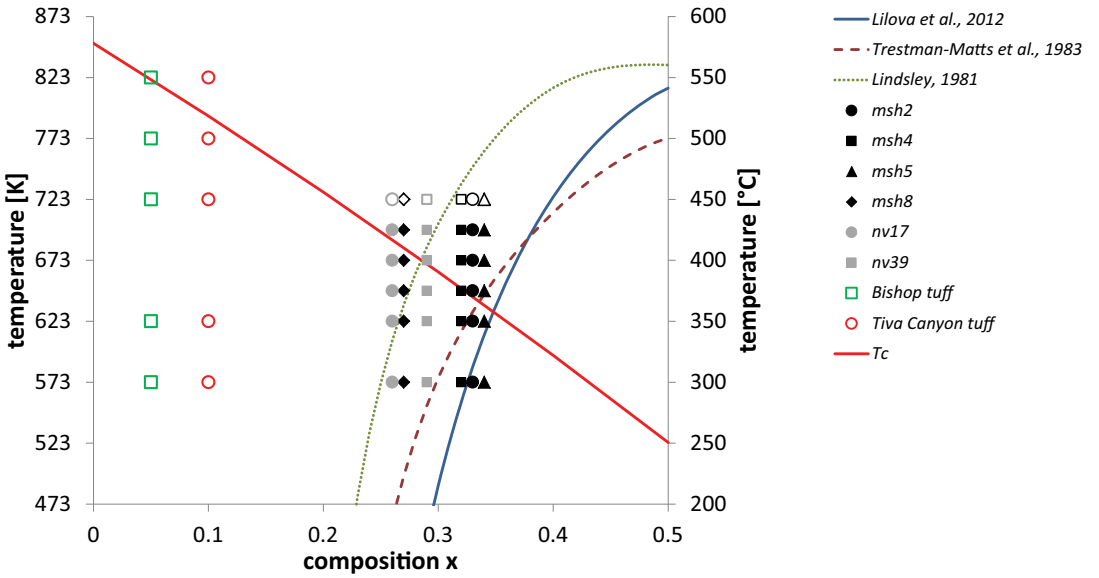

Figure 13. Summary of experimental annealing conditions and results. Solid and open symbols, respectively, indicate changes in $T_{C,heating}$ of greater than and less than 15°C for long-period treatments (>100 h). Binary solvus curves of *Lindsley* [1981], *Trestman-Matts et al*. [1983], and *Lilova et al*. [2012] are shown for comparison. Significant changes in T_C appear to occur in a restricted area near or below the solvus curves, suggesting a possible role of unmixing (see text for details). The T_C(x) curve of *Bleil and Petersen* [1982] is also shown for reference; interaction of magnetic ordering and cation ordering may be significant in these samples.

of electrons rather than of entire cations. The disequilibrium cation distributions postulated by *Bowles et al*. [2013] therefore appear to require either (a) that intersite ferrous-ferric electron transfer is slowed significantly by the presence of Ti, Al, and Mg; or (b) that these nonmagnetic cations have site occupancies that are dependent on thermal history, and that their rearrangement can significantly affect the Curie temperature. Because the saturation magnetization at room temperature and at 10 K is unchanged by thermal treatments [*Bowles et al*., 2013], we must discard the idea of *A-B* Fe^{2+}-Fe^{3+} reordering (assuming collinear antiferromagnetic ordering), and thus we suppose that the cation reordering model must involve changing site occupancies of Al and Mg, or perhaps a short-range ordering mechanism operating within the octahedral sublattice [*Wechsler et al*., 1984; *Moskowitz*, 1987; *Carter-Stiglitz et al*., 2006]. We will return to this idea below.

Either of the two candidate mechanisms above (unmixing/rehomogenization and cation ordering/disordering) involves a redistribution of metal cations within the titanomagnetites; the difference is primarily one of length scale and therefore also of time scale. *A-B* site exchange operates on sub-nanometer scales; spinodal unmixing has characteristic length scales on the order of 10 nm; and nucleation and growth of near-end-member lamellae requires migration of cations over distances on the order of 100 nm [e.g., *Harrison and Putnis*, 1999a]. As with thermal diffusion, chemical diffusion operates on timescales that vary according to the square of the length scale involved, and thus unmixing is necessarily orders of magnitude slower than intersite exchange. Previous experimental work [e.g., *Price*, 1981b] indicates that cation diffusion is much too slow to cause production and reabsorption of end-member exsolution lamellae in the time-temperature ranges where we observe significant increases (hours to months at 350°C–400°C) and decreases (minutes at 450°C–500°C) in T_C. *Price* [1981b] found that the characteristic homogenization time for sub-100 nm magnetite-ulvöspinel lamellae was approximately 2500 h at 500°C. Moreover the low-*T* susceptibility data (Figure 8) show no evidence for the production of a Ti-rich exsolved phase, as would be expected if nucleation and growth were proceeding during annealing at moderate temperatures.

Spinodal decomposition is harder to rule out via rate arguments, but it too is inconsistent with the observed thermomagnetic behavior, specifically the homogeneity of Curie temperature in almost all postannealing thermomagnetic runs. Sinusoidal variations in composition, initially of small amplitude and growing in time, would produce a broadening of the d*k*/d*T* minima defining T_C, as the initial single value for the homogeneous phase becomes a distribution of values corresponding to the nonuniform compositional range. As the

process continues, any inflated T_C originating in Fe-enriched volumes would necessarily be paired with an accompanying deflated T_C from the Fe-depleted regions. Our observations show unambiguously that in most cases, the increase in T_C occurs homogeneously throughout the volume of the titanomagnetites in each specimen during annealing below 425°C: there is no indication of multiple Curie temperatures for the homogeneous phase on the heating run, and the derivative peaks invariably become sharper as T_C increases (Figure 7a) [see *Bowles et al*., 2013, Figure 3].

It is also worth pointing out that the crest of the binary magnetite-ulvöspinel solvus is raised to temperatures hundreds of degrees higher by the presence of significant amounts of substituted Mg and Al [*Bowles et al*., 2012]. The strong apparent relationship between changing Curie temperatures and the binary solvus (Figure 13) may therefore be fortuitous. Moreover the lack of annealing effects on T_C in the purer magnetites of the Bishop and Tiva Canyon samples may be attributable to factors other than location above the solvus, including more rapid ferrous-ferric exchange kinetics. Both the chemical unmixing model and the cation ordering model have problems explaining some of our observations, but on balance we find that unmixing/rehomogenization is more problematic, and we therefore favor changing cation distributions in the spinel structure (or possibly within the octahedral sites alone) as the mechanism responsible for the observed thermomagnetic behavior.

The major unknown is how the cation distribution changes in a way that preserves the low-temperature spontaneous magnetization while changing the strength of the exchange interactions. One possibility is that the phenomena are driven by Al-Mg intersite exchange, which easily explains the constancy of M_S, and which may change T_C via lattice strain and accompanying changes in exchange coupling (R. Harrison, personal communication, 2013). Another conceivable mechanism involves short-range ordering of the cation distribution within the octahedral site, as several authors have speculated [*Wechsler et al*., 1984; *Moskowitz*, 1987; *Wanamaker and Moskowitz*, 1994]. *Carter-Stiglitz et al*. [2006] invoked low-temperature suppression of *B*-site electron hopping in titanomagnetites to explain various aspects of their magnetic behavior and Mössbauer spectra. Some form of charge ordering of the octahedral ferrous and ferric ions, or a segregation of *B*-site nonmagnetic ions, may conceivably affect the Curie temperature but would not alter the bulk spontaneous magnetization as long as antiferromagnetic *AB* interactions remain dominant. Recent atomistic models developed by *Harrison et al*. [2013] for cation ordering in the magnesioferrite-qandilite solid solution (an analog of the magnetite-ulvöspinel system in which the Fe^{2+} is entirely replaced by Mg^{2+}) show a strong tendency toward short-range chemical clustering within the octahedral sublattice, on length scales of a few unit cells, at temperatures near the solvus. Such short-range order may well explain all of the key observations that we have made: progressive, homogeneous increases in T_C on annealing at subsolvus temperatures; rapid decreases in T_C above a critical temperature near the solvus; and room-temperature values of k and M_S that are virtually independent of thermal history (barring oxidation unmixing). Additional research using techniques such as XMCD [*Pattrick et al*., 2002; *Pearce et al*., 2010] is currently underway in an effort to characterize cation valencies and site occupancies [*Lappe et al*., 2014].

5.3. Temperature-Dependent Equilibrium Cation Distribution

The continuing increase in T_C with protracted heating in the isothermal annealing experiments, and the failure to reach a plateau even after 1000 h at temperatures between 350 and 425°C (Figure 9) indicate that the cation distribution has not reached the equilibrium state and that the degree of order is still increasing, driving T_C up to 500°C and beyond. Annealing at higher temperatures does not increase the Curie temperature in any of our samples, and the multicycle $k(T)$ experiments show that even brief exposure to temperatures above about 500°C is sufficient to cause significant disordering of the cation distribution, with accompanying reduction of T_C to ~375°C. Thus we infer that, if cation reordering is the principal mechanism of T_C enhancement, there must be a very sharp gradient in the $Q_{eq}(T)$ curve for these titanomagnetites between about 425°C and 500°C. For $T \leq 425$°C the equilibrium distribution is relatively ordered, with $T_C \geq 475$°C, whereas for $T \geq 500$°C the equilibrium distribution is much more disordered, having $T_C \leq 375$°. Continued reordering at temperatures above the "cation unblocking" (or closure) temperature of about 500°C is sufficiently rapid that the distribution reversibly follows the equilibrium curve, and the changes that occur at higher temperatures are not observable during subsequent cooling (e.g., see the multicycle $k(T)$ run in *Bowles et al*. [2013, Figure 2]). Reordering kinetics are slow enough for $T \leq 425$°C that we have been unable to reach equilibrium in any of our experiments at those temperatures. Thus we can say little about the details of the $Q_{eq}(T)$ function, other than that it evidently varies sharply between about 425°C

and 500°C to account for the large change (>100°C) in the equilibrium T_C over that small temperature interval. For comparison, the equilibrium order parameter for magnesioferrite changes slowly and smoothly between 400°C and 1000°C, with an accompanying 80° range of Curie temperatures (from 370°C to 290°C) over that 600°C range of equilibration temperatures [*Harrison and Putnis*, 1999b, 1999a].

One obvious suggestion is that this sharp change has to do with the interaction of magnetic ordering and cation ordering [*Harrison and Putnis*, 1997, 1999a; *Harrison et al*., 2013]. In these titanomagnetites, both phenomena happen in nearly the same temperature range (Figure 13), unlike magnesioferrite, where significant ordering and especially disordering occur on lab timescales at temperatures far above T_C. It also appears likely that subsolvus *B*-site chemical clustering [*Harrison et al*., 2013] plays a major role, as discussed in section 5.2 above. Dissipation of the chemical clustering above the solvus could readily account for the sharp changes we observe in the 425°C–500°C range (Figure 13).

5.4. Temperature and Composition-Dependent Cation Ordering Kinetics

Although our experimental data contain relatively little information on how the equilibrium cation distribution changes with temperature, they provide an essential picture of the temperature dependence of reordering timescales, which are accessible in laboratory experiments over a relatively narrow window from about 300°C–450°C. At lower temperatures, if cation reordering continues to occur, it is on timescales of months, years or longer. Certainly such timescales are available for slow cation ordering in nature, and it is possible that high degrees of order and elevated Curie temperatures may result, although we note that 30 years at ambient temperatures have produced no appreciable ordering in the surficial samples at site MSH12-08.

The process (schematically depicted in Figure 6) involves the essential ideas of a temperature-dependent equilibrium cation distribution and a temperature-dependent cation mobility which governs the rate of approach to the equilibrium distribution. These ideas have previously been used to explain similar phenomena in the magnesioferrite system [e.g., *Harrison and Putnis*, 1999b, 1999a] and in the magnetite-ulvöspinel system [*Lattard et al*., 2006]. According to this model, titanomagnetites in the magma chamber at 950–1000°C have the strongly disordered cation distributions that represent the equilibrium state for that temperature range. During the rapid initial cooling after eruption, quick rearrangement of cations allows the distribution to remain in equilibrium, and the degree of order increases accordingly. Eventually as the temperature continues falling, diffusion rates become too slow for the cation distribution to remain in equilibrium, and it "freezes in" a degree of order that depends on the cooling history (Figure 6a). Fast continuous cooling at shallow depths results in relatively disordered distributions and relatively low Curie temperatures, as in the surficial samples of site MSH12-08 (Figure 5). Deeper in the flow units, the quasi-isothermal post-emplacement interval and ensuing slower cooling result in more ordered distributions and elevated T_C (Figure 6a). These more ordered states are the ones responsible for the thermomagnetic irreversibility in the $k(T)$ runs: with increasing temperature, the frozen distribution reaches the equilibrium curve (Figure 6b) while cation mobility begins to increase. On continued heating, the distribution follows the equilibrium curve to more disordered states, and after the maximum temperature is attained, subsequent cooling at a rate much higher than the slow, natural, post-emplacement rate freezes in a relatively disordered distribution with a diminished T_C (Figure 6b). The isothermal annealing experiments drive the system around a clockwise path in the (T,Q) space, inflating T_C (Figure 6b).

A number of pioneering studies [e.g., *Bleil*, 1976; *O'Donovan and O'Reilly*, 1980; *Wechsler et al*., 1984] explored the possibility of producing variably ordered cation distributions by quenching from different high temperatures (exceeding 600°C), and the results generally showed little or no relation between quench temperature and magnetic properties (particularly M_S) that are sensitive to cation ordering. As pointed out by *Harrison and Putnis* [1999a], because these experiments all involved fast quench rates, they all follow essentially the same path in the *Q-T* diagram regardless of starting temperature (Figure 6): they follow the equilibrium curve down to the closure temperature for those fast cooling rates, and then freeze in the corresponding degree of order.

What is the significance of the evident difference between natural slow cooling (Figure 5; $dT_C/d(\log(t_{cool}))$ $\sim$ 42 for MSH8/MSH12-8) and laboratory isothermal annealing (Figures 9 and 10; $dT_C/d(\log(t_{soak}))$ $\sim$ 25 for MSH8 at 350°C) in producing the observed changes in T_C? We do not have a definite answer. It's certainly true that the experiments do not exactly duplicate the thermal histories and other conditions experienced

by the samples after emplacement. Annealing in air in the lab produces effects that are generally very similar to those produced by postemplacement "annealing," but the (presumably less oxic) conditions in the natural environment may play some role. We are currently carrying out annealing experiments in controlled atmospheres to investigate this. Natural cooling is also more continuous in time than the lab experiments, which involve abrupt cooling after extended isothermal annealing. Consequently t_{cool} is less precisely defined than t_{soak} and one might imagine that they are not really equivalent—the former is controlled by overburden thickness and its calculated values are model-dependent, whereas the latter is experimentally controlled. However, it is important to realize that none of the model parameters in equation (2) actually affect the slope: since $t_{cool}(z) = cz^2$ in the conductive cooling model, it follows that $dT_C/d(\log(t_{cool})) = {}^1/_2 dT_C/d(\log(z))$, and the slope in Figure 5b is determined directly by the variation of T_C with depth in Figure 5a. Changes in parameters such as diffusivity, emplacement temperature or $T(z, t_{cool})$ affect only the intercept values of the relation in Figure 5b, through their influence on the value of c. Thus the slope differences for natural slow cooling and laboratory annealing cannot be resolved by choosing different parameters in the conductive cooling model, and this remains as a significant question to be addressed in continuing research.

There is clearly a significant role of titanomagnetite composition in controlling the occurrence and kinetics of T_C evolution, although our data do not allow us to resolve the individual effects of Ti, Al, and Mg concentrations on the underlying process (Figures 12 and 13). Composition may play a direct role (e.g., slowing of ferrous-ferric exchange by increasing concentrations of other cations), and it also very likely plays an indirect role through its effects on T_C and on solvus temperature, which in turn may influence bulk cation ordering and short-range chemical ordering. Our results show that the rate of increase in T_C is systematically larger in the more Ti-, Al-, and Mg-rich titanomagnetites, especially for annealing temperatures of 350°C–375°C (Figure 12a). These annealing temperatures are close to the magnetic ordering temperature and to published solvus temperatures for the composition range of our samples (Figure 13), and therefore models involving interaction of magnetic and cation ordering or octahedral-site chemical clustering in the vicinity of the solvus provide attractive explanations. Additional $T_C(T_{soak}, t_{soak})$ data for higher-x samples will help to clarify the dependence of kinetics on composition, as well as constraining the crystal-chemical mechanisms responsible. Ongoing work is focusing on synthetic titanomagnetites of varying controlled compositions, to systematize the individual and combined effects of the key metal components Ti, Al, and Mg [e.g., *Lappe et al*., 2013, 2014].

5.5. Implications

As pointed out by *Bowles et al* [2013], time and temperature-dependent cation distributions and the resultant evolving Curie temperatures in volcanic titanomagnetites have a number of important geophysical consequences. Most obviously and directly, there are complications in the use of T_C to estimate titanomagnetite compositions, but perhaps more importantly there are major ramifications in paleomagnetism and potential applications in geospeedometry.

Acquisition, retention, and demagnetization of partial thermoremanence and thermoviscous remanence, both in nature and in the laboratory, may all be significantly affected by cation reordering and changes in T_C. Quantitative models of the time, temperature, and field-dependent evolution of magnetization are essentially all based on Néel theory, and in such models it is a fundamental assumption that T_C is a material constant and that the function $M_S(T)$ is single-valued and invariant for any mineral, governing not only magnetization intensities but also the scaling of temperature-dependent anisotropies and energy-barrier distributions [e.g., *Dunlop and West*, 1969; *Dodson and McClelland-Brown*, 1980; *Walton*, 1980; *Dunlop*, 1984; *Winklhofer et al*., 1997; *Fabian*, 2000; *Lanci and Kent*, 2003; *Shcherbakov and Fabian*, 2005; *Jackson et al*., 2006; *Egli*, 2009]. When T_C is in fact a function of thermal history, and especially when it can be changed by heating at $T < T_C$, thermomagnetic behavior is correspondingly altered in ways that can be expected to strongly affect paleointensity estimates and paleomagnetic paleothermometry [*McClelland-Brown*, 1981; *Middleton and Schmidt*, 1982; *Dunlop et al*., 1997a, 1997b, 2000; *McClelland et al*., 2004; *Yu and Dunlop*, 2006; *Paterson et al*., 2010]. Such effects may be most important in samples like ours, with titanomagnetites having compositions near $x' = 0.3$. With increasing x', T_C decreases and solvus temperatures are thought to increase (Figure 13), so if the latter do in fact play an important role in the phenomenon, the most significant changes may be expected to occur at $T > T_C$ for higher x'.

Among the pioneering studies of cation distributions in titanomagnetites, a major concern was the possibility of self-reversal caused by a shift from *B*-site dominance ($M_B > M_A$) to *A*-site dominance as a result of slow

ordering over long time scales [e.g., *Verhoogen*, 1956; *Creer and Stephenson*, 1972]. Because we find no significant change in saturation magnetization at low or ambient temperatures, the kind of reordering we have observed seems very unlikely to produce such self-reversal of primary remanence.

A potential geological application of time and temperature-dependent cation ordering in titanomagnetites is in geospeedometry. Geospeedometers based on cation ordering in silicates have been developed for orthopyroxene [*Ganguly*, 1982], alkali feldspars [*Kroll and Knitter*, 1991], olivine [*Redfern et al*., 1996], and amphibole [*Seifert and Virgo*, 1975]. They all exploit the fact that the degree of cation order is dependent not only on equilibration temperature, but on the entire thermal history of the sample. Once the temperature-dependent rate constant and the temperature-independent, structure-specific coefficients are quantified, a measured degree of order can be modeled in terms of emplacement temperature and cooling rate [e.g., *Harrison and Putnis*, 1999a]. The key advantage in using titanomagnetite over silicate systems lies in the fact that Curie temperature is a fast and easy measurement to make whereas diffraction studies are time-consuming. Such a cation-ordering based geospeedometer would be distinctly different from, and complementary to the proposed titanomagnetite geospeedometer of *Mollo et al*. [2013], which uses chemical composition (Fe, Ti, Al, and Mg) to quantify cooling rate over the temperature interval 1100–1000°C. Compositional controls on reordering kinetics (Figure 12) are an important aspect of potential applications in geospeedometry, and a better understanding of them will be essential.

6. Summary and Conclusions

Titanomagnetite-bearing pyroclastic samples from Mt St Helens and from Novarupta exhibit the following distinctive traits: (1) thermomagnetic runs for most samples exhibit one or two distinct magnetic phases, with respective Curie temperatures of 325°C–475°C and 540°C–580°C; (2) reflected-light microscopy shows that the susceptibility contributions of the low-T_C and high-T_C phases respectively correspond to the proportions of homogeneous and oxyexsolved titanomagnetites; (3) the higher Curie temperatures are observed primarily in samples from sites with estimated emplacement temperatures exceeding 600°C; (4) thermomagnetic cooling curves are very similar for different samples from each flow unit, but heating curves are more variable and commonly indicate Curie temperatures for the homogeneous titanomagnetites that are higher than those seen in the cooling curves, in some cases by more than 100°C; (5) the thermomagnetic irreversibility increases systematically as a function of depth in an individual pyroclastic cooling unit; (6) multicycle thermomagnetic runs show that brief exposure to temperatures exceeding 450°C or 500°C causes the Curie temperatures of the homogenous titanomagnetites to revert to a narrow range of values near 375°C and reduces or eliminates the irreversibility; (7) isothermal annealing at temperatures between 300°C and 425°C for time intervals between 0.3 and 1000 h causes the Curie temperatures of the homogenous titanomagnetites to increase, in proportion with the logarithm of annealing time; (8) the rate at which T_C increases is generally related to titanomagnetite composition; over the range in our samples ($0.25 < x' < 0.35$) the increases are most rapid in samples with more substitution, although we cannot determine the individual roles of the various cation species; and (9) there is little permanent change caused in the samples by repeated cycles of increasing T_C by moderate-temperature annealing and then decreasing it by exposure to higher temperatures in thermomagnetic runs.

These observations are best explained in terms of time and temperature dependence of the cation distribution in the homogeneous titanomagnetites [*Bowles et al*., 2013], perhaps involving short-range ordering within the *B* sites. Reordering timescales are experimentally accessible in a relatively narrow temperature window from about 300°C to 450°C. At higher temperatures the distribution is presumably more random and the Curie temperature lower than those that we observe, but reordering is so fast during cooling to the closure temperature of 500°C that no record of the higher-*T* state is preserved. This closure temperature is expected to be rate-dependent, but in our $k(T)$ experiments the cooling rate is fixed at 10°–15°/min.

Below 300°C reordering rates are too slow to produce any measurable effects on laboratory timescales up to 1000 h, but on geological timescales slow rearrangement of the cation distribution may conceivably produce very large changes in the Curie temperature of titanomagnetites in thick extrusive units or in intrusive rocks. Because this process may occur at temperatures near or even below the initial Curie temperature of the titanomagnetites, the mechanisms of remanence acquisition and stabilization can potentially be substantially influenced by cation reordering.

Acknowledgments

This work was supported by National Science Foundation grants EAR-0944067 and EAR-1315845 (to J.A.B. and M.J.J.) and EAR-0943999 (to Jeff Gee) and through support from the NSF Instruments and Facilities program for the Institute for Rock Magnetism. Samples were collected at the Katmai National Park with permission from the National Park Service and under permit KATM-2010-SCI-0014. Samples were collected at Mt. St. Helens National Monument under permit MSH-17-2010 and MSH-07-2012. Samples used in this research are registered with unique identifiers (IGSN) through geosamples.org. All rock magnetic data presented in this paper are available from the Magnetics Information Consortium (MagIC) database (earthref.org/MAGIC/). Other data are available by e-mailing J. Bowles. We thank Subir Banerjee, Bruce *Moskowitz*, Richard Harrison, Joshua Feinberg, and Jeff Gee for insightful discussions, and Jason Steindorf, John Bowar, Jesse Vavrek, and Amanda Flynn-Stach for their help in sample collection. Perceptive reviews by Richard Harrison and Dominique Lattard helped improve both our understanding and our presentation of the results. This is IRM contribution 1407.

References

Banks, N. G., and R. P. Hoblitt (1981), Summary of temperature studies of 1980 deposits, in *The 1980 Eruptions of Mount St. Helens, Washington, U.S. Geol. Surv. Prof. Pap.*, vol. 1250, edited by P. W. Lipman and D. R. Mullineaux, pp. 295–314, U.S. Geol. Surv., Washington, D. C.

Banks, N. G., and R. P. Hoblitt (1996), Direct temperature measurements of deposits, Mount St. Helens, Washington, 1980–1981, *U.S. Geol. Surv. Prof. Pap.*, *1387*, 83.

Bleil, U. (1976), Experimental-study of titanomagnetite solid-solution series, *Pure Appl. Geophys.*, *114*(2), 165–175, doi:10.1007/BF00878943.

Bleil, U., and N. Petersen (1982), Magnetic properties of natural minerals, in *Landolt-Börnstein: Zahlenwerte und Funktionen aus Naturwissensschaft und Technik, Neue Serie V, Band 1b*, edited by G. Angenheister, pp. 308–365, Springer, Heidelberg, Germany.

Bosi, F., U. Halenius, and H. Skogby (2009), Crystal chemistry of the magnetite-ulvospinel series, *Am. Mineral.*, *94*(1), 181–189, doi:10.2138/am.2009.3002.

Bowles, J. A., L. Tatsumi-Petrochilis, J. E. Hammer, and S. A. Brachfeld (2012), Multi-component cubic oxide exsolution in synthetic basalts: Temperature dependence and implications for magnetic properties, *J. Geophys. Res.*, *117*, B03202, doi:10.1029/2011JB008867.

Bowles, J. A., M. Jackson, T. S. Berquó, P. A. Sølheid, and J. S. Gee (2013), Inferred time- and temperature-dependent cation ordering in natural titanomagnetites, *Nat. Commun.*, *4*, 1916, doi:10.1038/ncomms2938.

Burton, B. P. (1991), The interplay of chemical and magnetic ordering, *Rev. Mineral.*, *25*, 303–321.

Burton, B. P., P. Robinson, S. A. McEnroe, K. Fabian, and T. B. Ballaran (2008), A low-temperature phase diagram for ilmenite-rich compositions in the system Fe_2O_3-$FeTiO_3$, *Am. Mineral.*, *93*(8–9), 1260–1272.

Carter-Stiglitz, B. S., B. Moskowitz, P. Solheid, T. S. Berquó, M. Jackson and A. Kosterov (2006), Low-temperature magnetic behavior of multi-domain titanomagnetites: TM0, TM16, and TM35, *J. Geophys. Res.*, *111*, B12S05, doi:10.1029/2006JB004561.

Chevallier, R., J. Bolfa, and S. Mathieu (1955), Titanomagnétites et ilménites ferromagnétiques, *Bull. Soc. Fr. Minéral. Cristallogr.*, *78*, 307–346.

Christiansen, R. L., and D. W. Peterson (1981), Chronology of the 1980 eruptive activity, in *The 1980 Eruptions of Mount St. Helens, Washington, U.S. Geol. Surv. Prof. Pap.*, vol. 1250, edited by P. W. Lipman and D. R. Mullineaux, pp. 17–30, U.S. Geol. Surv., Washington, D. C.

Creer, K. M., and A. Stephenson (1972), Some consequences of aluminum and magnesium impurities in naturally occurring titanomagnetites, *J. Geophys. Res.*, *77*(20), 3698–3710, doi:10.1029/JB077i020p03698.

Dodson, M. H., and E. McClelland-Brown(1980), Magnetic blocking temperatures of single-domain grains during slow cooling, *J. Geophys. Res.*, *85*(B5), 2625–2637, doi:10.1029/JB085iB05p02625.

Dunlop, D. J. (1984), Temperature, time, and interaction effects in rock magnetism, *J. Magn. Magn. Mater.*, *45*, 107–112.

Dunlop, D. J., and Ö. Özdemir (1997), *Rock Magnetism: Fundamentals and Frontiers, Cambridge Studies in Magnetism*, vol. 573, Cambridge Univ. Press, Cambridge, U. K.

Dunlop, D. J., and Ö. Özdemir (2007), Magnetization in rocks and minerals, in *Geomagnetism, Treatise Geophys.*, vol. 5, edited by M. Kono, pp. 277–336, Elsevier, Amsterdam.

Dunlop, D. J., and G. West (1969), An experimental evaluation of single-domain theories, *Rev. Geophys.*, *7*(4), 709–757.

Dunlop, D. J., Ö. Özdemir, and P. W. Schmidt (1997a), Paleomagnetism and paleothermometry of the Sydney Basin: 2. Origin of anomalously high unblocking temperatures, *J. Geophys. Res.*, *102*(B12), 27,285–27,295.

Dunlop, D. J., P. W. Schmidt, O. Ozdemir, and D. A. Clark (1997b), Paleomagnetism and paleothermometry of the Sydney Basin: 1. Thermoviscous and chemical overprinting of the Milton Monzonite, *J. Geophys. Res.*, *102*(B12), 27,271–27,283.

Dunlop, D. J., O. Ozdemir, D. A. Clark, and P. W. Schmidt (2000), Time-temperature relations for the remagnetization of pyrrhotite (Fe_7S_8) and their use in estimating paleotemperatures, *Earth Planet. Sci. Lett.*, *176*(1), 107–116.

Egli, R. (2009), Magnetic susceptibility measurements as a function of temperature and frequency I: Inversion theory, *Geophys. J. Int.*, *177*, 395–420.

Engelmann, R., A. Kontny, and D. Lattard (2010), Low-temperature magnetism of synthetic Fe-Ti oxide assemblages, *J. Geophys. Res.*, *115*, B12107, doi:10.1029/2010JB000865.

Evans, B. W., S. Bruno, and S. M. Kuehner (2006), Experimental determination of coexisting iron-titanium oxides in the systems FeTiAlO, FeTiAlMgO, FeTiAlMnO, and FeTiAlMgMnO at 800 and 900 degrees C, 1–4 kbar, and relatively high oxygen fugacity, *Contrib. Mineral. Petrol.*, *152*(2), 149–167, doi:10.1007/s00410-006-0098-z.

Evans, M. E., and F. Heller (2003), *Environmental Magnetism: Principles and Applications of Environmagnetics*, Academic, Amsterdam.

Fabian, K. (2000), Acquisition of thermoremanent magnetization in weak magnetic fields, *Geophys. J. Int.*, *142*(2), 478–486.

Fierstein, J., and W. Hildreth (1992), The Plinian Eruptions of 1912 at Novarupta, Katmai-National-Park, Alaska, *Bull. Volcanol.*, *54*(8), 646–684, doi:10.1007/BF00430778.

Fierstein, J., and C. J. N. Wilson (2005), Assembling an ignimbrite: Compositionally defined eruptive packages in the 1912 Valley of Ten Thousand Smokes ignimbrite, Alaska, *Geol. Soc. Am. Bull.*, *117*(7–8), 1094–1107, doi:10.1130/B25621.1.

Ganguly, J. (1982), Mg-Fe order-disorder in ferromagnesian silicates: II. Thermodynamics, kinetics and geological applications, in *Advances in Physical Geochemistry*, vol. 2, edited by S. K. Saxena, pp. 58–99, Springer, Berlin.

Gee, J. S., and D. V. Kent (2007), Source of oceanic magnetic anomalies and the geomagnetic polarity timescale, in *Geomagnetism, Treatise Geophys.*, vol. 5, edited by G. Schubert, pp. 455–507, Elsevier, Amsterdam.

Gee, J. S., Y. Yu, and J. Bowles (2010), Paleointensity estimates from ignimbrites: An evaluation of the Bishop Tuff, *Geochem. Geophys. Geosyst. 11*, Q03010, doi:10.1029/2009GC002834.

Ghiorso, M. S., and B. W. Evans (2008), Thermodynamics of rhombohedral oxide solid solutions and a revision of the Fe-Ti two-oxide geothermometer and oxygen-barometer, *Am. J. Sci.*, *308*(9), 957–1039, doi:10.2475/09.2008.01.

Grunder, A. L., D. Laporte, and T. H. Druitt (2005), Experimental and textural investigation of welding: Effects of compaction, sintering, and vapor-phase crystallization in the rhyolitic Rattlesnake Tuff, *J. Volcanol. Geotherm. Res.*, *142*, 89–104.

Haggerty, S. E. (1991), Oxide textures—A mini-atlas, *Rev. Mineral.*, *25*, 137–220.

Hamdeh, H. H., K. Barghout, J. C. Ho, P. M. Shand, and L. L. Miller (1999), A Mössbauer evaluation of cation distribution in titanomagnetites, *J. Magn. Magn. Mater.*, *191*(1–2), 72–78, doi:10.1016/s0304-8853(98)00340-0.

Harrison, R. J., and A. Putnis (1997), The coupling between magnetic and cation ordering: A macroscopic approach, *Eur. J. Mineral.*, *9*(6), 1115–1130.

Harrison, R. J., and A. Putnis (1999a), The magnetic properties and crystal chemistry of oxide spinel solid solutions, *Surv. Geophys.*, *19*(6), 461–520, doi:10.1023/A:1006535023784.

Harrison, R. J., and A. Putnis (1999b), Determination of the mechanism of cation ordering in magnesioferrite ($MgFe_2O_4$) from the time- and temperature-dependence of magnetic susceptibility, *Phys. Chem. Miner.*, *26*(4), 322–332, doi:10.1007/s002690050192.

Harrison, R. J., E. J. Palin, and N. Perks (2013), A computational model of cation ordering in the magnesioferrite-qandilite ($MgFe_2O_4$-Mg_2TiO_4) solid solution and its potential application to titanomagnetite (Fe_3O_4-Fe_2TiO_4), *Am. Mineral.*, *98*(4), 698–708, doi:10.2138/am.2013.4318.

Hildreth, W. (1987), New perspectives on the eruption of 1912 in the valley of ten thousand smokes, Katmai National Park, Alaska, *Bull. Volcanol.*, *49*(5), 680–693, doi:10.1007/BF01080359.

Hildreth, W., and J. Fierstein (2000), Katmai volcanic cluster and the great eruption of 1912, *Geol. Soc. Am. Bull.*, *112*(10), 1594–1620, doi:10.1130/0016-7606(2000)112<1594:kvcatg>2.0.co;2.

Hildreth, W., and J. Fierstein (2012), Eruptive history of Mount Katmai, Alaska, *Geosphere*, *8*(6), 1527–1567, doi:10.1130/GES00817.1.

Hunt, C. P., B. M. Moskowitz and S. K. Banerjee (1995), Magnetic properties of rocks and minerals, in *A Handbook of Physical Constants*, vol. 3, edited by T. J. Ahrens, pp. 189–204, AGU, Washington, D. C.

Jackson, M., B. Carter-Stiglitz, R. Egli, and P. Solheid (2006), Characterizing the superparamagnetic grain distribution $f(V,H_k)$ by thermal fluctuation tomography, *J. Geophys. Res.*, *111*, B12S07, doi:10.1029/2006JB004514.

Jensen, S. D., and P. N. Shive (1973), Cation distribution in sintered titanomagnetites, *J. Geophys. Res.*, *78*(35), 8474–8480.

Kakol, Z., J. Sabol, and J. M. Honig (1991), Cation distribution and magnetic-properties of titanomagnetites $Fe_{3-x}Ti_xO_4$(0£x<1), *Phys. Rev. B*, *43*(1), 649–654.

Kawabata, H., T. Hanyu, Q. Chang, J.-I. Kimura, A. R. L. Nichols, and Y. Tatsumi (2011), The petrology and geochemistry of St. Helena Alkali Basalts: Evaluation of the oceanic crust-recycling model for HIMU OIB, *J. Petrol.*, *52*, 791–838.

Kienle, J. (1991), Depth of the ash flow deposit in the Valley of 10000 Smokes, Katmai National Park, Alaska, *Geophys. Res. Lett.*, *18*(8), 1533–1536, doi:10.1029/91GL01186.

Kroll, H., and R. Knitter (1991), Al, Si exchange kinetics in sanidine and anorthoclase and modeling of rock cooling paths, *Am. Mineral.*, *76*(5–6), 928–941.

Kuntz, M. A., P. D. Rowley, N. S. Macleod, R. L. Reynolds, L. A. McBroome, A. M. Kaplan, and D. J. Lidke (1981), Petrography and particle-size distribution of pyroclastic-flow, ash-cloud, and surge deposits, in *The 1980 Eruptions of Mount St. Helens, Washington, U.S. Geol. Surv. Prof. Pap.*, vol. 1250, edited by P. W. Lipman and D. R. Mullineaux, pp. 525–539, U.S. Geol. Surv., Washington, D. C.

Kuntz, M. A., P. D. Rowley, and N. S. MacLeod (1990), Geologic map of pyroclastic flow and related deposits of the 1980 eruptions of Mount St. Helens, Washington, *U.S. Geol. Surv. Misc. Geol. Invest. Map*, *I-1950*.

Lagroix, F., S. K. Banerjee, and M. Jackson (2004), Magnetic properties of the Old Crow tephra: Identification of a complex iron titanium oxide mineralogy, *J. Geophys. Res.*, *109*, B01104, doi:10.1029/2003JB002678.

Lanci, L., and D. V. Kent (2003), Introduction of thermal activation in forward modeling of hysteresis loops for single-domain magnetic particles and implications for the interpretation of the Day diagram, *J. Geophys. Res.*, *108*(B3), 2142, doi:10.1029/2001JB000944.

Lappe, S.-C. L. L., J. Bowles, and M. Jackson (2013), *Time- and temperature-dependent cation ordering in synthetic Mg- and Al-substituted titanomagnetites, Abstract GP53B-1131 presented at 2013 Fall Meeting*, AGU, San Francisco, Calif.

Lappe, S.-C. L. L., J. Bowles, M. Jackson, and D. Keavney (2014), *XMCD and magnetic evidence for cation reordering in synthetic Mg- and Al-substituted titanomagnetites, Abstract GP33B-06 presented at Fall Meeting*, AGU, San Francisco, Calif.

Lattard, D., U. Sauerzapf, and M. Kasemann (2005), New calibration data for the Fe-Ti oxide thermo-oxybarometers from experiments in the Fe-Ti-O system at 1 bar, 1,000–1,300 degrees C and a large range of oxygen fugacities, *Contrib. Mineral. Petrol.*, *149*(6), 735–754, doi:10.1007/s00410-005-0679-2.

Lattard, D., R. Engelmann, A. Kontny, and U. Sauerzapf (2006), Curie temperatures of synthetic titanomagnetites in the Fe-Ti-O system: Effects of composition, crystal chemistry, and thermomagnetic methods, *J. Geophys. Res.*, *111*, B12S28, doi:10.1029/2006JB004591.

Lattard, D., U. Sauerzapf, and A. Kontny (2012), Rapid surficial oxidation of synthetic Fe-Ti oxides at high temperature: Observations and consequences for magnetic measurements, *Geochem. Geophys. Geosyst.*, *13*, Q08Z46, doi:10.1029/2012GC004152.

Lilova, K. I., C. I. Pearce, C. Gorski, K. M. Rosso, and A. Navrotsky (2012), Thermodynamics of the magnetite-ulvospinel (Fe_3O_4-Fe_2TiO_4) solid solution, *Am. Mineral.*, *97*(8–9), 1330–1338.

Lindsley, D. H. (1981), Some experiments pertaining to the magnetite-ulvospinel miscibility gap, *Am. Mineral.*, *66*(7–8), 759–762.

Lipman, P. W., and D. R. Mullineaux (Eds.) (1981), The 1980 eruptions of Mount St. Helens, Washington, *U.S. Geol. Surv. Prof. Pap.*, *1250*, 844.

Liu, Q. S., A. P. Roberts, J. C. Larrasoana, S. K. Banerjee, Y. Guyodo, L. Tauxe and F. Oldfield (2012), Environmental magnetism: Principles and applications, *Rev. Geophys.*, *50*, RG4002, doi:10.1029/2012RG000393.

Martín-Hernández, F., C. M. Lüneburg, C. Aubourg, and M. Jackson (Eds.) (2004), *Magnetic Fabric: Methods and Applications, Geol. Soc. Spec. Publ.*, vol. 238, 551 pp., The Geol. Soc. of London, London, U. K.

McClelland, E., C. J. N. Wilson, and L. Bardot (2004), Palaeotemperature determinations for the 1.8-ka Taupo ignimbrite, New Zealand, and implications for the emplacement history of a high-velocity pyroclastic flow, *Bull. Volcanol.*, *66*(6), 492–513.

McClelland-Brown, E. (1981), Paleomagnetic estimates of temperatures reached in contact metamorphism, *Geology*, *9*, 112–116.

Melson, W. G., and C. A. Hopson (1981), Preeruption temperatures and oxygen fugacitites in the 1980 eruptive sequence, in *The 1980 Eruptions of Mount St. Helens, Washington, U.S. Geol. Surv. Prof. Pap.*, vol. 1250, edited by P. W. Lipman and D. R. Mullineaux, pp. 641–648, U.S. Geol. Surv., Washington, D. C.

Middleton, M. F., and P. W. Schmidt (1982), Paleothermometry of the Sydney basin, *J. Geophys. Res.*, *87*(B7), 5351–5359.

Mollo, S., K. Putirka, G. Iezzi, and P. Scarlato (2013), The control of cooling rate on titanomagnetite composition: Implications for a geospeedometry model applicable to alkaline rocks from Mt. Etna volcano, *Contrib. Mineral. Petrol.*, *165*(3), 457–475, doi:10.1007/s00410-012-0817-6.

Moore, J. G., P. W. Lipman, D. A. Swanson, and T. R. Alpha (1981), Growth of lava domes in the crater, June 1980-January 1981, in *The 1980 Eruptions of Mount St. Helens, Washington, U.S. Geol. Surv. Prof. Pap.*, vol. 1250, edited by P. W. Lipman and D. R. Mullineaux, pp. 541–548, U.S. Geol. Surv., Washington, D. C.

Moskowitz, B. M. (1987), Towards resolving the inconsistencies in characteristic physical-properties of synthetic titanomaghemites, *Phys. Earth Planet. Inter.*, *46*(1–3), 173–183, doi:10.1016/0031-9201(87)90180-4.

Moskowitz, B. M., M. Jackson and C. Kissel (1998), Low-temperature magnetic behavior of titanomagnetites, *Earth Planet. Sci. Lett.*, *157*(3–4), 141–149.

Néel, L. (1948), Propriétés magnétiques des ferrites: Ferrimagnétisme et antiferromagnétisme, *Ann. Phys. Paris*, *3*, 137–198.

Néel, L. (1955), Some theoretical aspects of rock magnetism, *Adv. Phys.*, *4*, 191–243.

Nishitani, T. (1981), Magnetic properties of titanomagnetites containing spinel ($MgAl_2O_4$), *J. Geomagn. Geoelectr.*, *33*, 171–179.

O'Donovan, J. B., and W. O'Reilly (1980), Temperature-dependent cation distribution in titanomagnetites—Experimental test, *Phys. Chem. Mineral.*, *5*(3), 235–243.

O'Neill, H. S. C., and A. Navrotsky (1983), Simple spinels; crystallographic parameters, cation radii, lattice energies, and cation distribution, *Am. Mineral.*, *68*(1–2), 181–194.
O'Neill, H. S. C., and A. Navrotsky (1984), Cation distributions and thermodynamic properties of binary spinel solid-solutions, *Am. Mineral.*, *69*(7–8), 733–753.
O'Neill, H. S. C., H. Annersten, and D. Virgo (1992), The temperature-dependence of the cation distribution in magnesioferrite ($MgFe_2O_4$) from powder XRD structural refinements and Mössbauer-spectroscopy, *Am. Mineral.*, *77*(7–8), 725–740.
O'Reilly, W. (1984), *Rock and Mineral Magnetism*, Blackie Acad. and Prof., London, U. K.
O'Reilly, W., and S. K. Banerjee (1965), Cation distribution in titanomagnetites (1-x) Fe_3O_4-x Fe_2TiO_4, *Phys. Lett.*, *17*, 237–238.
Olhoeft, G. R., R. L. Reynolds, J. D. Friedman, G. R. Johnson, and G. R. Hunt (1981), Physical properties of the June 1980 dacite dome, in *The 1980 eruptions of Mount St. Helens, Washington, U.S. Geol. Soc. Prof. Pap.*, vol. 1250, edited by P. W. Lipman and D. R. Mullineaux, pp. 549–556, U.S. Geol. Soc., Washington, D. C.
Özdemir, Ö., and W. O'Reilly (1982), An experimental study of the intensity and stability of thermoremanent magnetization acquired by synthetic monodomain titanomagnetite substituted by aluminum, *Geophys. J. R. Astron. Soc.*, *70*, 141–154.
Palmer, H. C., W. D. MacDonald, C. S. Gromme, and B. B. Ellwood (1996), Magnetic properties and emplacement of the Bishop tuff, California, *Bull. Volcanol.*, *58*(2), 101–116.
Paterson, G. A., A. P. Roberts, C. Mac Niocaill, A. R. Muxworthy, L. Gurioli, J. G. Viramonte, C. Navarro, and S. Weider (2010), Paleomagnetic determination of emplacement temperatures of pyroclastic deposits: An under-utilized tool, *Bull. Volcanol.*, *72*(3), 309–330, doi:10.1007/s00445-009-0324-4.
Pattrick, R. A. D., G. Van Der Laan, C. M. B. Henderson, P. Kuiper, E. Dudzik, and D. J. Vaughan (2002), Cation site occupancy in spinel ferrites studied by X-ray magnetic circular dichroism: Developing a method for mineralogists, *Eur. J. Mineral.*, *14*(6), 1095–1102, doi:10.1127/0935-1221/2002/0014-1095.
Pearce, C. I., C. M. B. Henderson, N. D. Telling, R. A. D. Pattrick, J. M. Charnock, V. S. Coker, E. Arenholz, F. Tuna, and G. van der Laan (2010), Fe site occupancy in magnetite-ulvöspinel solid solutions: A new approach using X-ray magnetic circular dichroism, *Am. Mineral.*, *95*(4), 425–439, doi:10.2138/am.2010.3343.
Price, G. D. (1981a), Subsolidus phase-relations in the titanomagnetite solid-solution series, *Am. Mineral.*, *66*(7–8), 751–758.
Price, G. D. (1981b), Diffusion in the titanomagnetite solid-solution series, *Mineral. Mag.*, *44*(334), 195–200, doi:10.1180/minmag.1981.044.334.13.
Purucker, M., and K. Whaler (2007), *Crustal Magnetism, in Geomagnetism, Treatise Geophys.*, vol. 5, edited by G. Schubert, pp. 195–237, Elsevier, Amsterdam.
Redfern, S., C. Henderson, B. Wood, R. Harrison, and K. Knight (1996), Determination of olivine cooling rates from metal-cation ordering, *Nature*, *381*(6581), 407–409.
Richards, J. C. W., J. B. O'Donovan, Z. Hauptman, W. O'Reilly, and K. M. Creer (1973), A magnetic study of titanomagnetite substituted by magnesium and aluminium, *Phys. Earth Planet. Inter.*, *7*(4), 437–444, doi:10.1016/0031-9201(73)90023-X.
Riehle, J. R. (1973), Calculated compaction profiles of rhyolitic ash-flow tuffs, *Geol. Soc. Am. Bull.*, *84*, 2193–2216.
Rosenbaum, J. G. (1993), Magnetic grain-size variations through an ash-flow sheet: Influence on magnetic properties and implications for cooling history, *J. Geophys. Res.*, *98*(B7), 11,715–711,727.
Rosenbaum, J. G., and R. B. Waitt (1981), Summary of eyewitness accounts of the May 18 eruption, in *The 1980 Eruptions of Mount St. Helens, Washington, U.S. Geol. Surv. Prof. Pap.*, vol. 1250, edited by P. W. Lipman and D. R. Mullineaux, pp. 53–68, U.S. Geol. Surv., Washington, D. C.
Rowley, P. D., M. A. Kuntz, and N. S. Macleod (1981), Pyroclastic-flow deposits, in *The 1980 Eruptions of Mount St. Helens, Washington, U.S. Geol. Surv. Prof. Pap.*, vol. 1250, edited by P. W. Lipman and D. R. Mullineaux, pp. 489–512, U.S. Geol. Surv., Washington, D. C.
Saito, T., N. Ishikawa, and H. Kamata (2004), Iron-titanium oxide minerals in block-and-ash-flow deposits: Implications for lava dome oxidation processes, *J. Volcanol. Geotherm. Res.*, *138*(3–4), 283–294.
Schlinger, C. M., D. R. Veblen, and J. G. Rosenbaum (1991), Magnetism and magnetic mineralogy of ash flow tuffs from Yucca Mountain, Nevada, *J. Geophys. Res.*, *96*(B4), 6035–6052.
Seifert, F. A., and D. Virgo (1975), Kinetics of the Fe2+-Mg, order-disorder reaction in anthophyllites: Quantitative cooling rates, *Science*, *188*(4193), 1107–1109.
Shcherbakov, V. P., and K. Fabian (2005), On the determination of magnetic grain-size distributions of superparamagnetic particle ensembles using the frequency dependence of susceptibility at different temperatures, *Geophys. J. Inter.*, *162*(3), 736–746.
Sheridan, M. F., and D. M. Ragan (1976), Compaction of Ash-Flow Tuffs, in *Developments in Sedimentol*, vol. 2, edited by G. C. Amstutz, pp. 677–717, Elsevier, N. Y.
Stephenson, A. (1972), Spontaneous magnetization curves and Curie points of spinels containing two types of magnetic iron, *Philos. Mag.*, *25*(5), 1213–1232.
Tait, S., R. Thomas, J. Gardner, and C. Jaupart (1998), Constraints on cooling rates and permeabilities of pumice in an explosive eruption jet from colour and magnetic mineralogy, *J. Volcanol. Geotherm. Res.*, *86*(1–4), 79–91, doi:10.1016/S0377-0273(98)00075-4.
Tanaka, H., and Y. Yamamoto (2014), Microscopic observation of titanomagnetite grains during palaeointensity experiments of volcanic rocks, *Geophys. J. Int.*, *196*(1), 145–159, doi:10.1093/gji/ggt387.
Tauxe, L. (2010), *Essentials of Paleomagnetism*, 489 pp., Univ. of Calif. Press, Berkeley.
Trestman-Matts, A., S. E. Dorris, S. Kumarakrishnan, and T. O. Mason (1983), Thermoelectric determination of cation distributions in Fe_3O_4-Fe_2TiO_4, *J. Am. Ceram. Soc.*, *66*(12), 829–834, doi:10.1111/j.1151-2916.1983.tb10996.x.
Turcotte, D. L., and G. Schubert (1982), *Geodynamics*, 450 pp., John Wiley, N. Y.
Turner, M. B., S. J. Cronin, R. B. Stewart, M. Bebbington, and I. E. M. Smith (2008), Using titanomagnetite textures to elucidate volcanic eruption histories, *Geology*, *36*(1), 31–34.
Verhoogen, J. (1956), Ionic ordering and self-reversal of magnetization in impure magnetites, *J. Geophys. Res.*, *61*(2), 201–209, doi:10.1029/JZ061i002p00201.
Wallace, P. J., J. Dufek, A. T. Anderson, and Y. X. Zhang (2003), Cooling rates of Plinian-fall and pyroclastic-flow deposits in the Bishop Tuff: Inferences from water speciation in quartz-hosted glass inclusions, *Bull. Volcanol.*, *65*(2–3), 105–123, doi:10.1007/s00445-002-0247-9.
Walton, D. (1980), Time-temperature relations in the magnetization of assmblies of single-domain grains, *Nature*, *286*, 245–247.
Wanamaker, B. J., and B. M. Moskowitz (1994), Effect of nonstoichiometry on the magnetic and electrical-properties of synthetic single-crystal $Fe_{2.4}Ti_{0.6}O_4$, *Geophys. Res. Lett.*, *21*(11), 983–986, doi:10.1029/94GL00877.

Wechsler, B. A., D. H. Lindsley, and C. T. Prewitt (1984), Crystal-structure and cation distribution in titanomagnetites ($Fe_{3-X}Ti_XO_4$), *Am. Mineral.*, *69*(7–8), 754–770.

Winklhofer, M., K. Fabian, and F. Heider (1997), Magnetic blocking temperatures of magnetite calculated with a three-dimensional micromagnetic model, *J. Geophys. Res.*, *102*(B10), 22,695–22,709.

Worm, H.-U., and M. Jackson (1999), The superparamagnetism of Yucca Mountain Tuff, *J. Geophys. Res.*, *104*(B11), 25,415–425,425.

Yu, Y. J., and D. J. Dunlop (2006), Testing the independence of partial thermoremanent magnetizations of single-domain and multidomain grains: Implications for paleointensity determination, *J. Geophys. Res.*, *111*, B12S31, doi:10.1029/2006JB004434.

Zies, E. G. (1924), Hot springs of the Valley of Ten Thousand Smokes, *J. Geol.*, *32*, 303–310.